

NACA RM E56K10

C.1

NACA

RESEARCH MEMORANDUM

DESIGN AND EXPERIMENTAL INVESTIGATION OF A SINGLE-
STAGE TURBINE WITH A DOWNSTREAM STATOR

By Henry W. Plohr, Donald E. Holeski, and Robert E. Forrette

Lewis Flight Propulsion Laboratory
Cleveland, Ohio

CLASSIFICATION CHANGED

UNCLASSIFIED

LIBRARY COPY

FEB 1 1957

LANGLEY AERONAUTICAL LABORATORY
LIBRARY NACA
LANGLEY FIELD, VIRGINIA

To

By authority of Dir. PA 3 E. H. ...
Date 12-3-58
NB 3-2-59

CLASSIFIED DOCUMENT

This material contains information affecting the National Defense of the United States within the meaning of the espionage laws, Title 18, U.S.C., Secs. 793 and 794, the transmission or revelation of which in any manner to an unauthorized person is prohibited by law.

NATIONAL ADVISORY COMMITTEE FOR AERONAUTICS

WASHINGTON
January 25, 1957

UNCLASSIFIED



3 1176 01436 0854

NATIONAL ADVISORY COMMITTEE FOR AERONAUTICS

RESEARCH MEMORANDUM

DESIGN AND EXPERIMENTAL INVESTIGATION OF A SINGLE-STAGE TURBINE

WITH A DOWNSTREAM STATOR

By Henry W. Plohr, Donald E. Holeski, and Robert E. Forrette

SUMMARY

The use of a high-work-output single-stage turbine with a downstream stator in preference to a conventional two-stage turbine appears to be desirable for certain turbojet-engine designs. In order to determine the performance of such a turbine, a cold-air turbine was designed and experimentally investigated.

The turbine as designed did not produce design work because of higher losses in the rotor than anticipated in design. When the upstream-stator throat area was reduced by 4 percent, the turbine produced the equivalent design work of 22.31 Btu per pound at equivalent design blade tip speed of 522 feet per second with an over-all rating efficiency of 0.830 and a weight flow 2 percent less than design. The maximum efficiency at equivalent design speed was 0.857.

For almost the whole range of turbine operation, the downstream stator was effective in turning the flow out of the rotor back to the axial direction. At design work and blade speed the energy of the whirl component of velocity at the rotor exit corresponded to 5.7 percent in turbine efficiency. The downstream stator recovered 71 percent of this energy, corresponding to 4.0 percent in turbine efficiency. The downstream-stator performance was considered to be good whenever there was a fair amount of negative whirl to recover at the rotor exit.

INTRODUCTION

The limitations imposed on turbojet engines for high flight speeds by the turbine component have been the subject of previous analytical investigations at the NACA Lewis laboratory. The range of engine design-point operation for engines having conventional one- and two-stage turbines (turbines without downstream stators) is analyzed in reference 1. Reference 2, which is a similar investigation for one-stage turbines with downstream stators, concludes that the improvement in capacity of

UNCLASSIFIED



4108

CM-1

this type turbine over that of conventional high-output one-stage turbines is sufficiently large to warrant the use of such a turbine for certain engine applications. Also, when the turbine requirements can be met by both a conventional two-stage turbine and a single-stage machine having downstream stators, the latter unit has the mechanical advantage in applications requiring turbine blade cooling. For certain engine designs, it may also be true that the use of a single-rotor turbine would result in a lighter weight engine.

The successful use of this type of turbine design naturally depends upon whether the turbine will attain experimentally the performance assumed in the analysis of reference 2. The rotor aerodynamic limits used were considered critical because of the high subsonic rotor hub entrance Mach numbers, large rotor turning angles, and near-limiting-loading rotor-exit whirl. In some cases the downstream-stator aerodynamics was considered critical because of the high subsonic stator-entrance Mach numbers and high turning angles. By using a quasi-three-dimensional rotor design technique and available transonic-compressor design information to design the downstream stator, it appeared possible that the assumed performance might be attained.

In order to determine whether a turbine of this type will yield satisfactory performance, an experimental turbine was fabricated and investigated with cold-air inlet conditions. The turbine, having a single row of downstream-stator blades, was designed to drive a hypothetical transonic compressor at high flight Mach numbers. The purpose of this report is (1) to present the over-all performance results of the experimental tests, and (2) to evaluate the performance of the downstream stator in terms of its effect on over-all turbine performance. In addition, a brief description of the engine analysis, as well as the turbine and blade profile design analysis, is presented herein. The experimental performance results are presented for a range of blade speed at turbine pressure ratios up to that giving limiting turbine work.

SYMBOLS

- A area, sq ft
- a local velocity of sound, $\sqrt{\gamma gRT}$
- a'_{cr} critical velocity, $\sqrt{\frac{2\gamma}{\gamma+1} gRT}$
- D diffusion factor, $\left(1 - \frac{V_{4,h}}{V_{3,h}}\right) + \frac{-V_{u,3,h}}{2\sigma_h V_{3,h}}$
- g gravitational constant, 32.174 ft/sec²

- 4108
- CM-1 back
- Δh turbine work, Btu/lb
- M Mach number
- p pressure, lb/sq ft
- p_x^i rating total pressure, static pressure plus velocity pressure corresponding to axial component of velocity, lb/sq ft
- R gas constant, 53.35 ft-lb/(lb)(°R)
- \mathcal{R} recovery factor, $(\ln p_{x,4}^i/p_{x,3}^i)/(\ln p_3^i/p_{x,3}^i)$
- r radius
- T temperature, °R
- U blade speed, ft/sec
- V absolute velocity, ft/sec
- W relative velocity, ft/sec
- w weight flow, lb/sec
- α absolute flow angle, angle between air velocity and axial direction, deg
- γ ratio of specific heats ($\gamma_{sl} = 1.4$)
- δ ratio of total pressure to NACA standard sea-level pressure of 2116 lb/sq ft

e function of $\gamma, \frac{\gamma_{sl}}{\gamma} \left[\frac{\left(\frac{\gamma+1}{2} \right)^{\frac{\gamma}{\gamma-1}}}{\left(\frac{\gamma_{sl}+1}{2} \right)^{\frac{\gamma_{sl}}{\gamma_{sl}-1}}} \right]$

- η adiabatic efficiency

θ_{cr} squared ratio of critical velocity to critical velocity at NACA standard sea-level conditions, $\frac{\frac{2r}{\gamma + 1} gRT^1}{\frac{2r_{sl}}{\gamma_{sl} + 1} gRT_{sl}^1}$

σ solidity, ratio of chord to spacing

τ torque, ft-lb

$\bar{\omega}$ total-pressure-loss coefficient, $\frac{1 - \frac{p_4^1}{p_3^1}}{1 - \left[\frac{1}{1 + \frac{\gamma-1}{2}(M_{3,h})^2} \right]^{\frac{\gamma}{\gamma-1}}}$

Subscripts:

h hub

m mean

sl NACA standard sea-level conditions ($T_{sl} = 518.7^\circ \text{R}$)

t tip

te trailing edge

u tangential component or direction

x axial component or direction

O flight conditions

1,1a,2, measuring stations (see fig. 10)
3,4,5

Superscripts:

' absolute stagnation state

" relative stagnation state

TURBINE DESIGN

Engine Design Analysis

In order to select a turbine configuration that is typical of the type under consideration, a brief engine gas-generator analysis preceded the final choice of the turbine design point. The compressor and turbine components used in the analysis were selected with the aid of the turbine chart, figure 5(b) of reference 2, in the following manner. Assuming an engine temperature ratio of 3.0, a flight Mach number in the stratosphere of 2.8, and a downstream-stator diffusion factor of 0.4, the chart indicates that a turbine having a blade centrifugal stress of 30,000 pounds per square inch and a hub-tip radius ratio of 0.7 would drive a compressor with a pressure ratio of about 3.5 and an equivalent weight flow of about 20 pounds per second per square foot of frontal area. A hypothetical transonic-compressor map was then chosen. The choice was based on the preceding compressor requirements at the high flight Mach number as well as on the need for sufficient compressor operating range for engine operation at the lower flight Mach numbers. The engine operating line chosen is shown on the compressor map in figure 1.

The mode of engine operation chosen was one of constant engine rotational speed from the highest flight Mach number ($M_0 = 2.8$) down to that Mach number ($M_0 = 1.136$) at which compressor aerodynamics limits the engine speed. In this manner, turbine stress was the limiting factor at the high flight speeds, while the compressor imposed the limit at the lower flight Mach numbers in the stratosphere. At takeoff, the turbine stress was again the limiting factor. There is a possibility that rotating stall within the compressor might limit operation at the highest flight Mach number. This would reduce the flight Mach number range of satisfactory engine operation but in no way affect the turbine design requirements for purposes of this design analysis.

The 3023° R turbine-inlet temperature used in the analysis presumed the use of an air-cooled turbine. The engine cycle was penalized with compressor bleed for cooling purposes at flight Mach numbers below 2.0, but the turbine was not charged with cooling-air pumping work or losses due to mixing of the cooling air with the working fluid. At higher flight speeds it was assumed that ram air could do the necessary cooling. The major assumptions that went into the final engine analysis and the resulting turbine requirements are listed in table I. The maximum equivalent turbine work required was chosen as the design work for the subject turbine.

██████████

Cold-Air-Turbine Velocity Diagrams

The design requirements for the subject turbine are:

Equivalent turbine work, $\Delta h/\theta_{cr,1}$, Btu/lb	22.31
Equivalent specific weight flow, $w\sqrt{\theta_{cr,1}}\epsilon/A_t\delta_1$, (lb/sec)/sq ft . .	10.5
Equivalent blade tip speed, $U_t/\sqrt{\theta_{cr,1}}$, ft/sec	522

The following assumptions were used in establishing the turbine velocity diagrams:

- (1) Ratio of specific heats γ of 1.4
- (2) Free-vortex distribution of whirl velocity
- (3) Simple radial equilibrium
- (4) Hub-tip radius ratio r_h/r_t of 0.7
- (5) Diffusion factor at hub of downstream stator D_h of 0.4
- (6) Total-pressure loss across upstream stator p_2'/p_1' of 0.983
- (7) Adiabatic efficiency across rotor η of 0.90
- (8) Downstream-stator total-pressure-loss coefficient $\bar{\omega}$ of 0.05.

Transonic-compressor stator data (fig. 6 of ref. 3) were used to aid the choice of the downstream-stator loss coefficient for the assigned value of stator hub-radius diffusion factor of 0.4. The free-stream velocity diagrams as well as the velocity diagrams in the plane of the rotor and upstream-stator trailing edges are shown in figure 2. The velocities in the plane of the trailing edge were computed from the free-stream diagrams assuming continuity of flow and zero total-pressure loss between the two stations. The blockage area in the plane of the trailing edge was determined from the blade profiles discussed in the following section of this report.

It is interesting to note the critical aerodynamic flow conditions imposed on the turbine as a result of choosing this particular engine operating point. The rotor has a hub inlet Mach number of 0.833 and must turn the flow through 110.6° . The rotor-exit axial Mach number is 0.694 at the mean radius, indicating that the rotor is near limiting loading (ref. 4). The downstream-stator hub inlet Mach number is 0.846, and the design flow turning angle at this radius is 34.32° .

██████████

CONT#

Blade Profile Design

With the velocity diagrams specified, the upstream-stator and rotor blade shapes were designed and the downstream-stator blade surface velocities were calculated, using a quasi-three-dimensional flow analysis for determining the blade surface velocity distribution at three turbine radii (hub, mean, and tip). The downstream-stator blade profile was determined by using accepted compressor blade design techniques.

Design analysis. - The method of obtaining the blade surface velocities was considered to be quasi three-dimensional because the analysis of the flow was divided into two parts, a two-dimensional blade-to-blade solution at three radii, and an axisymmetric solution in the radial-axial plane. The axisymmetric solution was obtained by using a mean stream surface, which was considered to be that surface comprising the midchannel lines of the three radial blade profile elements. The midchannel line at any radius was located midway along velocity-potential lines between the convex and concave surfaces of the blade profile. The blade surface velocities and the velocity on the midchannel line were related assuming a linear variation of streamline curvature along velocity-potential lines between adjacent blade surfaces (ref. 5). The radial variation of velocity on the mean stream surface was assumed to satisfy the conditions of simplified radial equilibrium.

These criteria establish the relation between the velocities in the three-dimensional field bounded by the blade surfaces. If a variation of total pressure and temperature is assumed throughout the field, the absolute magnitude of the velocities can be established and the mass flow thus determined with the aid of the stream-filament charts of reference 5. The flow network that was assumed in calculating the blade surface velocities was checked for irrotationality (ref. 5) before the solution was considered complete. The blade surface velocities on that portion of the blade suction surface not in the blade channel were estimated from the required average suction-surface velocity, the velocity diagrams, and the channel velocity solution, where the required average suction-surface velocity was determined by considering the flow to be irrotational between the free-stream velocity diagrams and the channel-bounding velocity-potential line.

For the upstream stator and the rotor, the radial variation of mass flow, as well as the radial variation of midchannel tangential velocity, was specified. Assuming a blade profile shape at any radius establishes the entire blade shape, and the design problem becomes one of finding that shape. For both blade rows, the absolute midchannel tangential velocity was specified to be free-vortex in nature. A linear variation of the stream-filament mass-flow parameter (μ_{n_0} , ref. 5) with axial distance from the entrance to the exit of each blade row established continuity of

flow through the blade passage and the radial variation of mass flow for a specified set of velocity diagrams. It also establishes an assumption of linear total-pressure loss with axial distance.

Number of blades. - An arbitrary choice of approximately $1\frac{1}{4}$ inches for the axial chord, along with the solidity considerations of reference 6, resulted in a choice of 40 blades for the upstream stator and 74 blades for the rotor of the 15-inch-tip-diameter test facility.

The solidity of the downstream stator was established from the chosen diffusion factor at the hub, the design vector diagrams, and the following definition of the diffusion factor:

$$D_h = \left(1 - \frac{V_{4,h}}{V_{3,h}} \right) + \frac{-V_{u,4,h}}{2\sigma_h V_{3,h}}$$

Using this solidity and an actual chord of 1.25 inches, 50 downstream-stator blades were chosen for the same turbine tip diameter.

Upstream stator. - With the preceding assumptions and conditions, a trial stator hub profile converging to a throat at the channel exit was assumed. The throat opening was set so that it would pass the required mass flow with a sonic midchannel velocity. A slight curvature on the suction surface was assumed downstream of the throat. The calculated surface velocities shown in figure 3(a) were deemed acceptable, since the flow velocities accelerated along the suction surface.

With the hub profile specified, the velocity vectors on the mean stream surface were thereby established, and the shape of the mean and tip profiles were obtained by trial-and-error solution. The midchannel positions of the throats of all three blade sections were assigned to lie on a radial line. Thus, the assigned velocity vectors at the hub determined the blade throat midchannel velocity vectors at the other radii. The calculated blade surface velocity distributions for the mean- and tip-radius profiles are shown in figures 3(b) and (c), respectively. The surface velocities estimated from irrotationality considerations are also shown. The velocity peak and subsequent deceleration on the suction surface of the tip-radius profile are not considered desirable but were considered acceptable, since the deceleration occurred only at the tip-radius profile.

Rotor. - Several trial rotor hub profiles were assumed before the desired surface velocity distribution was attained. The rotor hub throat opening at the exit of the passage was set so that the midchannel velocity was sonic. A straight suction-surface profile was assumed downstream of the throat, thereby establishing the midchannel flow angle at the throat. The channel portion of the profile was adjusted until the desired sonic

velocity was attained on the suction surface. The choice of blade suction-surface profile upstream of the flow channel was determined by estimating the velocity distribution on it. The average velocity on this portion of the blade is determined by the amount of fluid turning that is done between the free-stream flow and the first velocity-potential line in the blade channel. A turning of 10° was used, providing an average surface critical velocity ratio of 0.935 on the suction surface between the leading edge and the first velocity-potential line. The assignment of a sonic throat velocity requires an expansion downstream of the throat to the relative supersonic exit velocity specified by the velocity diagrams. Since the blade is of the straight-backed type, this expansion will be of the type analyzed in reference 7. The surface velocity distribution of the hub-radius profile is shown in figure 4(a).

The mean- and tip-radius profiles were determined by trial-and-error solution for the blade shape. The centers of the throats at the channel exit for these two sections were set at the axial position where the calculated midchannel velocity was sonic. The surface velocities for these profiles are shown in figures 4(b) and (c), respectively. The slight diffusion that exists on the suction surface of both these profiles was not considered so undesirable as to warrant another trial. If these surface velocities were not acceptable, another hub-radius profile would have to be assumed, since only one blade shape will satisfy the flow conditions imposed by the hub profile under the existing assumptions.

Downstream stator. - The design flow conditions through the downstream stator of the subject turbine were very similar to flow conditions encountered in an experimental investigation of an axial-discharge stator operating behind a transonic-compressor rotor (ref. 8). Information presented in reference 8 was therefore used to determine the blade profile of the downstream stator at three radii. A double-circular-arc profile was chosen having a maximum thickness of 6 percent of the blade chord. The experimental results of reference 8 show the incidence angle for minimum loss for a circular-arc profile to be approximately 3° over a range of inlet Mach numbers. The turbine downstream-stator design incidence angle was therefore chosen as 3° , constant radially. Reference 8 showed that Carter's rule (ref. 9) for calculating deviation angle indicated good agreement between theory and experiment in the range of minimum-loss incidence angle. A trial-and-error solution of Carter's equation for deviation angle was used to obtain blade camber and deviation angles from the required turning and specified incidence angle and solidity. The turbine downstream-stator design therefore resulted in a profile having the following section profile characteristics (see fig. 1 of ref. 3):

Radius	Diffusion factor	Inlet Mach number	Camber angle, deg	Turning angle, deg	Deviation angle, deg
Hub	0.399	0.846	37.60	34.32	6.33
Mean	.366	.796	32.30	29.34	5.87
Tip	.344	.766	28.00	25.54	5.48

The blade surface velocity distribution for the downstream stator was determined by the basic method described in the design analysis section assuming a linear total-pressure loss with axial distance. The calculated velocities are presented in figure 5.

Blade profiles. - Scale drawings of the blade profiles at the hub, mean, and tip sections for all blade rows are shown in figure 6. The drawings are to scale for blade shape, blade solidity, and axial location of blade rows. The blade solidity and mean aspect ratio of all three blade rows based on the axial chord are as follows:

	Upstream stator	Rotor	Downstream stator
Hub solidity, σ_h	1.516	2.804	1.849
Mean solidity, σ_m	1.298	2.341	1.535
Tip solidity, σ_t	1.156	1.985	1.311
Mean aspect ratio, λ	1.731	1.775	1.830

The section coordinates used in fabricating the blade shapes are presented in table II. The geometrical difference between the flat-plate blade section required for blade fabrication and the cylindrical-surface design layout was taken into account in determining these coordinates. The difference was only significant for the hub- and mean-radius blade profile sections of the upstream stator.

EXPERIMENTAL APPARATUS

Test Installation

A 15-inch-tip-diameter turbine-component test facility was used to evaluate the performance of the subject turbine over a range of rotor speed and pressure ratio. Figure 7 shows the experimental turbine installation with the top half of the outer casing removed. The aluminum-bladed rotor is shown in figure 8. The blades of all three blade rows were stud-mounted so that the angular position could be adjusted.

The arrangement of the experimental equipment is shown in figure 9. Ambient air was drawn from the test cell through an electrostatic precipitator-type air filter and then heated by passing through a heat exchanger. The temperature of the air at the turbine inlet was maintained near 685° R by automatic temperature-control valves. This inlet temperature was high enough to avoid local water-saturated airflow conditions within the turbine. The airflow was measured by a calibrated flat-plate orifice installed in conformance with ASME specifications. The air was exhausted by the laboratory low-pressure exhaust system after passing through the turbine. A remotely controlled valve downstream of a surge tank in the low-pressure exhaust line was used to maintain the desired pressure ratio across the turbine.

The power output of the turbine was absorbed by an eddy-current type dynamometer that was cradle-mounted for torque measurements. The torque force measurement was made with a calibrated commercial pneumatic load cell. The rotational speed of the turbine was measured with an electronic counter that determined the average turbine rotational speed over a period of 1 second within 1 revolution per minute.

Instrumentation

A cross section of the experimental turbine showing the axial location of the instrumentation is presented in figure 10(a). The circumferential positions of the various instruments for all measuring stations are shown in figure 10(b). Typical instrument probes used in the investigation are shown in figure 11. The measurement of flow angle was made with two types of pressure-differential angle probes mounted in self-balancing angle-positioning actuators. The average angle of a radial traverse was tabulated as the flow angle. The pressures were measured with tetrabromoethane fluid manometers and were photographically recorded.

METHODS AND PROCEDURES

Experimental Procedure

Experimental data were taken at nominal values of inlet total to exit static-pressure ratio. At each pressure ratio, the turbine rotor speed was varied from 60 to 120 percent of design equivalent speed in 10-percent increments of speed. The turbine-inlet temperature was maintained between 683° and 687° R. The inlet total pressure varied between 1500 and 1700 pounds per square foot because of pressure losses in piping upstream of the turbine that depended on the airflow. At the equivalent design operating point, the inlet total pressure was about 1500 pounds per square foot, corresponding to a rotor Reynolds number of 201,000 based on average design mean-section rotor velocities.

Experimental Data Reduction and Performance Calculations

In order to evaluate the over-all turbine performance as well as that of the downstream stator, a calculated total pressure was used to determine the fluid total state as it passed through the turbine. This calculated total pressure was determined from measurements of static pressure, total temperature, and flow direction. A rating total pressure was also calculated in order to evaluate the energy involved in the tangential velocity component behind the rotor and the downstream stator. The ideal work of the turbine was based on these pressures and the measured inlet temperature. The actual turbine work was determined from torque, speed, and weight-flow measurements.

The calculated turbine total pressure at stations 1, 3, and 4 in the turbine annulus was determined from the following equation:

$$p' = p \left[\frac{1}{2} + \frac{1}{2} \sqrt{1 + \frac{2(\gamma - 1)}{\gamma} \frac{R}{g} \left(\frac{w\sqrt{T'}}{pA} \right)^2 \frac{1}{\cos^2 \alpha_x}} \right]^{\frac{\gamma}{\gamma - 1}} \quad (1)$$

This one-dimensional equation was derived from the equations of continuity and energy, the equation of state, and the isentropic relation between pressure and temperature. The static pressure used in this equation is the numerical average of hub and tip static pressures measured by the wall static-pressure taps at the axial station under consideration. The turbine weight flow used is that calculated from the orifice measurements, while the area is the measured annular area. The total temperature is determined by averaging the probe total-temperature readings (corrected for Mach number) at either station 1 or station 4. Temperature measurements at station 4 were also used in the total-pressure computation at station 3. The flow-angle measurements at stations 3 and 4 were plotted and faired against the static pressure at their respective stations. The faired flow-angle measurement is used in equation (1). The flow direction at station 1 is assumed to be axial.

In addition to this total-pressure computation at measuring stations 1, 3, and 4, a calculated turbine rating total pressure was computed at stations 3 and 4. This rating total pressure at a particular axial station is defined as the static pressure at that station plus the pressure corresponding to the axial component of velocity. This rating total pressure can be stated in equation form as

$$p'_x = p \left(1 + \frac{\gamma - 1}{2} M_x^2 \right)^{\frac{\gamma}{\gamma - 1}} \quad (2)$$

where M_x is the axial component of one-dimensional annulus Mach number. The axial Mach number used in equation (2) is calculated from the total pressure calculated by equation (1), the measured static pressure, and the faired flow-angle measurement. When this rating total pressure is defined as the turbine-exit pressure at station 3 or 4, the turbine is charged for the energy of the tangential component of velocity at that station.

The experimentally obtained equivalent torque and weight-flow data were plotted and faired against the over-all rating total-pressure ratio $p'_1/p'_{x,4}$ for lines of constant equivalent blade speed. The rotor speed control on the experimental turbine was sufficiently accurate so that data

were taken with the turbine operating within 1/10 of 1 percent of the desired blade speed. Information taken from the faired curves of torque and weight flow at even increments of the rating pressure ratio was used to compute the performance map.

Calculated values of p_1'/p_3' , $p_1'/p_{x,3}'$, and p_1'/p_4' were plotted and faired against $p_1'/p_{x,4}'$. The faired values of these calculated pressure ratios were used to compute the ideal work upon which the turbine efficiencies η_3 , $\eta_{x,3}$, and η_4 were based. These faired values of pressure ratio were also used to compute the downstream-stator recovery factor:

$$R = \frac{\ln \frac{p_{x,4}'}{p_{x,3}'}}{\ln \frac{p_3'}{p_{x,3}'}} \quad (3)$$

The downstream-stator recovery factor used in this report is derived in reference 10.

RESULTS AND DISCUSSION

The first experimental tests were made with the turbine blading as designed. The maximum turbine work output attained at design blade speed was 4 percent less than the design value. From the axial static-pressure distribution in the turbine annulus, it was determined that the upstream-stator-exit velocity was below the design value. This indicated that the stator-exit whirl was less than the design value, if it was assumed that the stator-exit flow angle was approximately equal to the design value. Since the exit of the rotor was designed to operate very near its limiting value of exit whirl, lower than design whirl at the rotor inlet was the primary reason the turbine did not produce design work at maximum pressure ratio.

In order to determine why the stator-exit velocity was below the design value, it is necessary to note first that the turbine was designed to have an unchoked upstream stator and a choked rotor at the design point. Reference 11 indicates that, for this type of turbine, the flow conditions between the rotor and upstream stator are controlled by the stator-exit flow angle and the effective rotor-to-stator throat area ratio at a given blade speed. The term "effective" rotor-to-stator throat area ratio is used to denote the fact that the actual area ratio must be modified by the total-pressure losses between the stator and rotor throats. Figure 10 of reference 11 indicates that a reduction in the ratio of

rotor-to-stator throat areas and/or an increase in stator-exit flow angle (as measured from the tangential flow direction) would result in a reduction in stator-exit whirl velocity for a given blade speed. For the subject turbine it was concluded that the apparent low value of stator-exit whirl was due to an effective rotor-to-stator throat area ratio less than design. Since the measured blade throat areas were equal to the design values, it was concluded that the subject turbine failed to produce design work because the losses in the rotor were higher than anticipated in design. The flow in the turbine compensated for this additional loss by increasing the relative total pressure to the rotor through a reduction in stator-exit whirl velocity.

In order to increase the experimental turbine work output to at least the design value, it was decided to change the actual rotor-to-stator throat area ratio. This could be accomplished by adjusting the angular position of either the rotor or stator blades. If the rotor throat area were thus increased, it was felt that the change in rotor blade channel dimensions upstream of the throat would tend to further increase the losses. In addition to this, the downstream stator would be required to pass a greater specific mass flow, which would probably choke the downstream stator and again limit the turbine work output. On the other hand, if the upstream-stator area were reduced, the losses in the stator upstream of the throat would probably not change, but the turbine would not pass design weight flow. The latter solution was chosen. In order to increase the turbine limiting work output to a value greater than the design value, reference 11 was used to estimate a required 4-percent decrease in upstream-stator flow area.

Over-All Performance

The experimental data obtained for the subject turbine with the upstream-stator area reduced 4 percent below the design value are shown in figures 12 to 14. The faired values of these data were used to obtain the over-all turbine performance map shown in figure 15. This figure is a plot of the equivalent turbine work $\Delta h/\theta_{cr}$ against the weight-flow - speed parameter $wU_t \epsilon / A_t \delta_1$ for constant values of equivalent blade speed and rating pressure ratio $p_1'/p_{x,4}'$. The efficiency contours shown charge the turbine with any exit whirl out of the downstream stators. The maximum work at design speed was 102 percent of design work. The choking weight flow through the turbine at the design point was 2 percent less than the design value as a result of reducing the stator area. The turbine rating efficiency at equivalent design work and blade speed was 0.830. A maximum rating efficiency of 0.857 was attained at design blade speed and at a turbine work output of about 80 percent of the design value.

Turbine Choking Characteristics

The subject turbine was designed to operate with the rotor as the choked blade row. The torque and weight-flow characteristics of the turbine presented in figures 13 and 14 can be used to determine that such was the case at equivalent design work and blade speed. Figure 14 shows that the turbine was choked for all blade speeds at rating total-pressure ratios greater than 2.25 (choking is indicated by no change in equivalent weight flow with rating total-pressure ratio for a given blade speed). At a rating total-pressure ratio (2.35) corresponding to equivalent design work, figure 14 also shows that the upstream stator was unchoked at equivalent design blade speed. This is indicated by the fact that the choking weight flow varies with blade speed in the vicinity of equivalent design blade speed. The fact that the equivalent torque for equivalent design blade speed increases as the rating pressure ratio is increased above that required to produce design work (fig. 13) indicates that the downstream stator was unchoked at the same operating point. This could not happen if the downstream stator were choked, since the change in pressure downstream of the stator could not be felt behind the rotor. Therefore, the conclusion is that the rotor was the choked blade row at the operating point corresponding to equivalent design work and blade speed.

A limit on the maximum work output of a single-stage turbine having downstream stators can be imposed by either choking in the downstream stator or limiting loading in the rotor. For the subject turbine, the pressure ratio at which the turbine work is limited can be determined from figure 13 for any blade speed investigated. With this information and the static-pressure distribution in the turbine annulus as a function of the turbine rating pressure ratio, it is possible to determine whether the turbine rotor limited the turbine work output before the downstream stator choked.

Figure 16(a) shows the variation of static pressure in the turbine annulus as a function of the rating total-pressure ratio for the lowest blade speed investigated. The torque data for this blade speed indicate that the turbine work was limited at pressure ratios greater than 2.27 (fig. 13). Figure 16(a) shows that the static pressure behind the rotor (station 3) decreased slightly as the turbine pressure ratio was increased above 2.27. This means that, at the lowest blade speed, the rotor reached limiting loading before the downstream stator choked. A similar trend is evident at 70- and 80-percent-design speeds (figs. 16(b) and (c)).

The same criterion cannot be used at the higher blade speeds (figs. 16(d) to (g)), because the limiting torque output occurs at or near the maximum calculated turbine rating pressure ratio. The static pressure behind the downstream stator dropped sharply as the pressure downstream of the turbine was lowered beyond that exhaust pressure which gave the

highest calculated pressure ratio $p_1'/p_{x,4}'$ across the turbine. This sharp drop in pressure was due to the fact that the downstream stator choked at some slightly lower pressure ratio and subsequently expanded downstream of this choked-flow area into supersonic flow. The calculated total pressure at the exit of the downstream stator for this type of operating point was not considered to be the correct turbine rating exit pressure, because it represented a decrease in rating pressure ratio with an increase in inlet total- to exit static-pressure ratio. These data points are shown in figure 16 without faired curves through the points. At 90, 100, 110, and 120 percent of design blade speed, the condition of choking in the downstream stators coincides with maximum turbine work output; therefore, it is not possible to determine from these data whether the turbine rotor limited the work output before the stator choked.

In order to determine whether the downstream stator limited the flow, experimental torque measurements were made without the downstream stator in place. These data indicated a slight increase in turbine limiting work at the two highest blade speeds, and it is therefore possible to conclude that the downstream stator limited the turbine work only at the two highest blade speeds.

Downstream-Stator Performance

The performance of the downstream stator of the subject turbine was analyzed from the calculated total pressures upstream and downstream of the stator. The effectiveness of the stator was analyzed with regard to the effect of the stator on over-all turbine performance and not on stator losses as such.

The turbine efficiencies based on the calculated total pressures ahead of and behind the downstream stator are shown in figure 17. The turbine efficiency η_3 was determined by using the calculated total pressure behind the rotor (station 3) for the ideal work. The turbine efficiency η_4 was determined in a similar manner from the calculated total pressure behind the downstream stator (station 4). The turbine rating efficiencies $\eta_{x,3}$ and $\eta_{x,4}$ were determined using the rating total pressures $p_{x,3}'$ and $p_{x,4}'$. The efficiency η_3 is always highest, since it does not include any total-pressure loss across the downstream stator and does not charge the rotor for the energy in the whirl component of rotor-exit velocity. The rating efficiency $\eta_{x,3}$ credits the turbine for the energy in the axial component of velocity and charges the turbine with the energy in the tangential component of velocity. It is therefore lower than η_3 , except when the absolute velocity out of the rotor is axial, when $\eta_{x,3}$ is equal to η_3 . The same criteria hold for the efficiency η_4 and the rating efficiency $\eta_{x,4}$ at station 4. For this

investigation the rating efficiency $\eta_{x,4}$ was essentially equal to the efficiency η_4 , because the measured flow angle out of the downstream stator was essentially axial for most of the range of turbine operation. The angle data taken downstream of the stator shown in figure 12(b) scatter within a band that is $\pm 2\frac{10}{2}$ from axial-flow direction except at very low work levels. The difference between η_4 and $\eta_{x,4}$ for an exit flow angle of $2\frac{10}{2}$ is negligible.

When the rating efficiency $\eta_{x,4}$ is greater than the rating efficiency $\eta_{x,3}$, the downstream stator is recovering more whirl energy than it loses in a total-pressure drop across the blade row. If the downstream stator recovered all the available whirl energy without itself incurring any loss, $\eta_{x,4}$ would be equal to η_3 . At design work and blade speed (fig. 17(e)), the turbine efficiency was 0.847 and the rating efficiency $\eta_{x,3}$ was 0.790. Thus, the whirl energy at the exit of the rotor corresponded to 5.7 percent in turbine efficiency. Downstream of the stator, the turbine rating efficiency $\eta_{x,4}$ was 0.830, the stator having recovered energy corresponding to 4.0 percent in turbine efficiency. The downstream stator thus had a total-pressure loss across the blade row corresponding to 1.7 percent in turbine efficiency at the design point.

In order to express the effectiveness of the downstream stator in recovering whirl energy while still taking into account the losses across the blade row, a downstream-stator recovery factor \mathcal{R} was computed. This recovery factor was first used to evaluate a turbine downstream stator in a similar type of investigation in reference 10. The recovery factor for the subject blade row is shown plotted in figure 18 for all turbine speeds investigated as a function of equivalent turbine work. A recovery factor corresponding to 1.0 indicates complete recovery of the energy in the whirl component at the rotor exit without any total-pressure loss across the downstream stator. A recovery factor of 0 indicates that the whirl energy recovered by the stator just equals the total-pressure loss across the blade row. A negative recovery factor indicates that the energy lost in a total-pressure drop across the downstream stator was higher than the whirl energy recovered by the blade row. Thus, the recovery factor can become negative if there is very little whirl energy available for the stator to recover and/or a high total-pressure loss across the downstream stator.

At design turbine work and speed, the recovery factor was 0.71, decreasing rapidly as the turbine work approached its limiting value because of an increase in total-pressure loss across the downstream stator. This increase in total-pressure loss is indicated by the rapid divergence of the η_3 and $\eta_{x,4}$ lines in figure 17(e) as the turbine work output is increased from the design value.

At design blade speed, a maximum recovery factor of 0.76 was attained at a turbine work of 20 Btu per pound, slightly below the design value. At turbine work outputs lower than 20 Btu per pound, the recovery factor dropped sharply, because the total-pressure loss across the blade row remained practically constant (compare the difference between η_3 and $\eta_{x,4}$ in fig. 17(e)) while the energy available for recovery rapidly decreased (compare the difference between $\eta_{x,3}$ and η_3). The recovery factor becomes zero when $\eta_{x,3}$ equals $\eta_{x,4}$ (see eq. (3)). The recovery factor was a large negative number at the lower work outputs mainly because of the large total-pressure loss across the stator. Figure 12(a) indicates that in this turbine operating range the stator is operating with a highly negative incidence angle, which is a possible reason for such high losses.

The variation of the stator recovery factor with turbine work is similar at the other blade speeds. In general, the range of turbine work for positive stator recovery factor decreased with increasing blade speed. The maximum value of the recovery factor at each blade speed also decreased with increasing blade speed.

The low value of the recovery factor at the two highest blade speeds is mainly due to the fact that the stator had little whirl energy to recover and was operating at a negative angle of incidence at all values of equivalent work. In general, the stator performance was considered good in the range of turbine operation where there was a fair amount of rotor-exit whirl energy for the stator to recover. The stator did introduce additional over-all turbine loss when it had little or no rotor-exit whirl energy to recover. For almost the whole range of turbine operation, the downstream stator was effective in turning the flow out of the rotor back to the axial-flow direction. This ability might be of importance in turbojet engines with afterburners where whirl at the entrance to the burner impairs engine performance.

SUMMARY OF RESULTS

The cold-air experimental investigation of a high-work-output single-stage turbine with a downstream stator yielded the following results:

1. The turbine as designed did not attain design work at design blade speed. This difficulty was attributed to higher losses in the rotor than anticipated in design. When the upstream-stator throat area was reduced 4 percent, the maximum turbine work at design blade speed was increased to 102 percent of design work.

2. At the equivalent design work output of 22.31 Btu per pound of airflow and the equivalent design blade tip speed of 522 feet per second, the modified turbine rating efficiency was 0.830. The maximum efficiency

was 0.857, occurring at design blade speed and a lower work output. At design work and blade speed, the turbine equivalent weight flow per unit frontal area was 2 percent lower than the design value of 10.5 pounds per second per square foot.

3. The turbine was designed to operate with the rotor as the choked blade row. These flow conditions were found to exist when the modified turbine was operated at design work and blade speed.

4. For almost the whole range of turbine operation, the downstream stator was effective in turning the flow out of the rotor back to the axial direction.

5. At design work and blade speed the energy of the whirl component of velocity at the rotor exit corresponded to 5.7 percent in turbine efficiency. The downstream stator recovered 71 percent of this energy, corresponding to 4.0 percent in turbine efficiency.

6. The downstream-stator performance was considered to be good whenever there was a fair amount of negative rotor-exit whirl to recover.

Lewis Flight Propulsion Laboratory
National Advisory Committee for Aeronautics
Cleveland, Ohio, November 14, 1956

REFERENCES

1. Cavicchi, Richard H., and English, Robert E.: Analysis of Limitations Imposed on One-Spool Turbojet-Engine Designs by Compressors and Turbines at Flight Mach Numbers of 0, 2.0, and 2.8. NACA RM E54F21a, 1954.
2. Cavicchi, Richard H., and Constantine, Anita B.: Analysis of Limitations Imposed on One-Spool Turbojet-Engine Designs by Turbines Having Down-Stream Stators at 0, 2.0, and 2.8 Flight Mach Numbers. NACA RM E54J14, 1955.
3. Lieblein, Seymour: Review of High-Performance Axial-Flow-Compressor Blade-Element Theory. NACA RM E53L22, 1954.
4. English, Robert E., Silvern, David H., and Davison, Elmer H.: Investigation of Turbines Suitable for Use in a Turbojet Engine with High Compressor Pressure Ratio and Low Compressor-Tip Speed. I - Turbine-Design Requirements for Several Engine Operating Conditions. NACA RM E52A16, 1952.

5. Huppert, M. C., and MacGregor, Charles: Comparison Between Predicted and Observed Performance of Gas-Turbine Stator Blade Designed for Free-Vortex Flow. NACA TN 1810, 1949.
6. Zweifel, O.: Optimum Blade Pitch for Turbo-Machines with Special Reference to Blades of Great Curvature. The Eng. Digest, vol. 7, no. 11, Nov. 1946, pp. 358-360; cont., vol. 7, no. 12, Dec. 1946, pp. 381-383.
7. Hauser, Cavour H., and Flohr, Henry W.: Two-Dimensional Cascade Investigation of the Maximum Exit Tangential Velocity Component and Other Flow Conditions at the Exit of Several Turbine-Blade Designs at Supercritical Pressure Ratios. NACA RM E51F12, 1951.
8. Sandercock, Donald M., Lieblein, Seymour, and Schwenk, Francis C.: Experimental Investigation of an Axial-Flow Compressor Inlet Stage Operating at Transonic Relative Inlet Mach Numbers. IV - Stage and Blade-Row Performance of Stage with Axial-Discharge Stators. NACA RM E54C26, 1954.
9. Carter, A. D. S.: The Low Speed Performance of Related Aerofoils in Cascade. Rep. No. R. 55, British N.G.T.E., Sept. 1949.
10. Davison, Elmer H., Petrash, Donald A., and Schum, Harold J.: Investigation of Turbines Suitable for Use in a Turbojet Engine with High Compressor Pressure Ratio and Low Compressor-Tip Speed. V - Experimental Performance of Two-Stage Turbine with Downstream Stator. NACA RM E55H16, 1955.
11. English, Robert E., and Cavicchi, Richard H.: One-Dimensional Analysis of Choked-Flow Turbines. NACA Rep. 1127, 1953. (Supersedes NACA TN 2810.)

TABLE I. - SUMMARY OF ENGINE DESIGN ANALYSIS

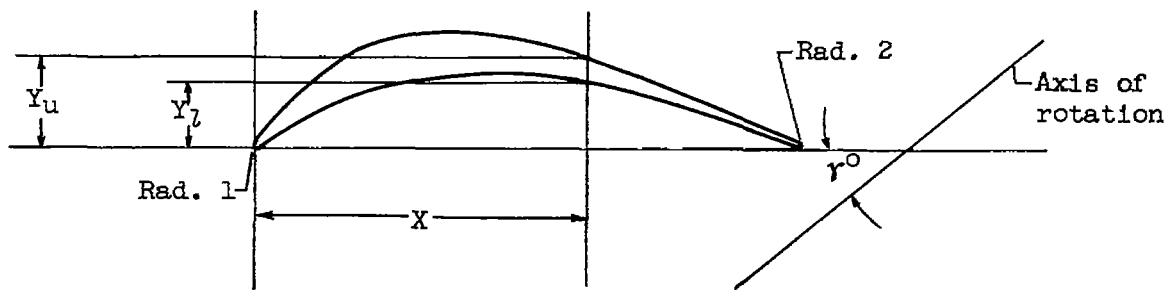
	Flight condition or flight Mach number					
	Takeoff	0.6	0.9	1.136	2.0	2.8
Equivalent turbine tip speed, ft/sec	522	482	502	522	522	522
Turbine centrifugal stress, psi	30,000	25,550	27,720	30,000	30,000	30,000
Equivalent turbine work, Btu/lb	22.06	19.98	21.15	22.31	21.98	21.60
Compressor bleed air for cooling, % compressor weight flow	7.5	7.5	7.5	7.5	0	0
Fuel-air ratio	0.0349	0.0371	0.0357	0.0351	0.0313	0.0265
Compressor equivalent rotational speed, % design	97.6	100	100	100	83.6	70
Compressor adiabatic efficiency	0.840	0.815	0.815	0.815	0.875	0.850
Compressor equivalent weight flow per unit frontal area, (lb/sec)/sq ft	34.14	35.00	35.00	35.00	27.68	20.19

Turbine-inlet temperature, °R	3023
Turbine hub-tip radius ratio	0.7
Ratio of tapered to untapered blade centrifugal stress	0.7
Ratio of specific heats for turbine	4/3
Total-pressure ratio across burner	0.95
Ratio of compressor to turbine tip-diameter area	0.99
Rotor blade material density, lb/cu ft	500
Air leakage between compressor and turbine, % compressor weight flow	1.5
Downstream-stator hub diffusion factor	0.4
Downstream-stator mean-radius solidity	1.5
Equivalent turbine weight flow per unit tip-diameter area, (lb/sec)/sq ft	10.5

TABLE II. - BLADE PROFILE COORDINATES

(a) Upstream-stator blade

[Rad. 1 = rad. 2 = 0.012".]

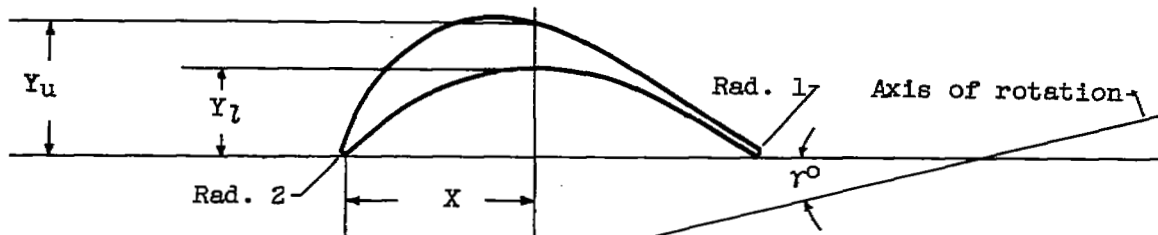


X	Blade coordinates, in.					
	Hub (diam., 10.50")		Mean (diam., 12.75")		Tip (diam., 15.00")	
	Y_l	Y_u	Y_l	Y_u	Y_l	Y_u
0	0.012	0.012	0.012	0.012	0.012	0.012
.1	.072	.160	.056	.128	.051	.113
.2	.140	.255	.118	.236	.116	.205
.3	.189	.320	.166	.310	.166	.281
.4	.223	.360	.201	.353	.205	.340
.5	.244	.382	.224	.377	.233	.377
.6	.257	.391	.238	.386	.251	.395
.7	.261	.388	.245	.384	.260	.394
.8	.259	.373	.244	.370	.262	.378
.9	.250	.351	.236	.345	.255	.353
1.0	.236	.323	.223	.313	.242	.322
1.1	.216	.289	.205	.278	.223	.286
1.2	.190	.251	.180	.240	.198	.246
1.3	.162	.212	.150	.199	.166	.204
1.4	.130	.173	.117	.158	.128	.161
1.5	.097	.133	.079	.114	.088	.117
1.6	.062	.093	.041	.070	.045	.073
1.7	.026	.053	-----	-----	-----	-----
1.714	-----	-----	.012	.012	-----	-----
1.719	-----	-----	-----	-----	.012	.012
1.781	.012	.012	-----	-----	-----	-----
r°	45°28'		40°58'		37°43'	

TABLE II. - Continued. BLADE PROFILE COORDINATES

(b) Rotor blade

[Rad. 1 = Rad. 2 = 0.012".]

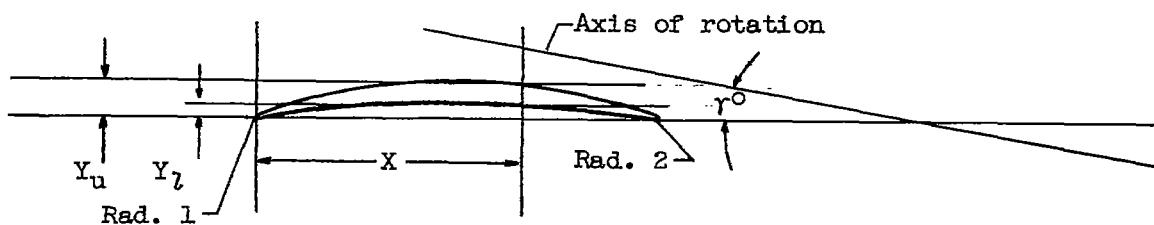


X	Blade coordinates, in.					
	Hub (diam., 10.50")		Mean (diam., 12.75")		Tip (diam., 15.00")	
	Y_l	Y_u	Y_l	Y_u	Y_l	Y_u
0	0.012	0.012	0.012	0.012	0.012	0.012
.1	.099	.193	.083	.230	.060	.238
.2	.193	.327	.159	.342	.119	.320
.3	.262	.423	.214	.407	.162	.363
.4	.311	.484	.254	.441	.191	.382
.5	.343	.514	.276	.449	.210	.384
.6	.355	.520	.285	.436	.220	.370
.7	.348	.498	.279	.404	.220	.342
.8	.322	.449	.258	.355	.208	.302
.9	.277	.373	.226	.294	.188	.255
1.0	.213	.276	.182	.228	.159	.204
1.1	.130	.173	.126	.160	.122	.154
1.2	.034	.070	.063	.092	.077	.104
1.251	.012	.012	-----	-----	-----	-----
1.3	-----	-----	.001	.025	.028	.054
1.308	-----	-----	.012	.012	-----	-----
1.368	-----	-----	-----	-----	.012	.012
r^0	2°21'		14°12'		22°41'	

TABLE II. - Concluded. BLADE PROFILE COORDINATES

(c) Downstream-stator blade

[Rad. 1 = Rad. 2 = 0.0075".]



X	Blade coordinates, in.					
	Hub (diam., 10.50")		Mean (diam., 12.75")		Tip (diam., 15.00")	
	Y_l	Y_u	Y_l	Y_u	Y_l	Y_u
0	0.0075	0.0075	0.0075	0.0075	0.0075	0.0075
.1	.020	.053	.016	.048	.013	.045
.2	.039	.086	.030	.077	.024	.071
.3	.053	.112	.042	.101	.034	.092
.4	.064	.131	.050	.117	.040	.107
.5	.070	.143	.055	.128	.044	.117
.6	.073	.148	.058	.133	.047	.122
.7	.073	.146	.057	.132	.046	.121
.8	.069	.139	.053	.125	.043	.114
.9	.061	.125	.048	.112	.038	.103
1.0	.049	.104	.038	.092	.031	.086
1.1	.033	.075	.026	.069	.021	.063
1.2	.013	.038	.010	.037	.008	.034
1.265	.0075	.0075	.0075	.0075	.0075	.0075
γ^0	12°32'		10°16'		8°34'	

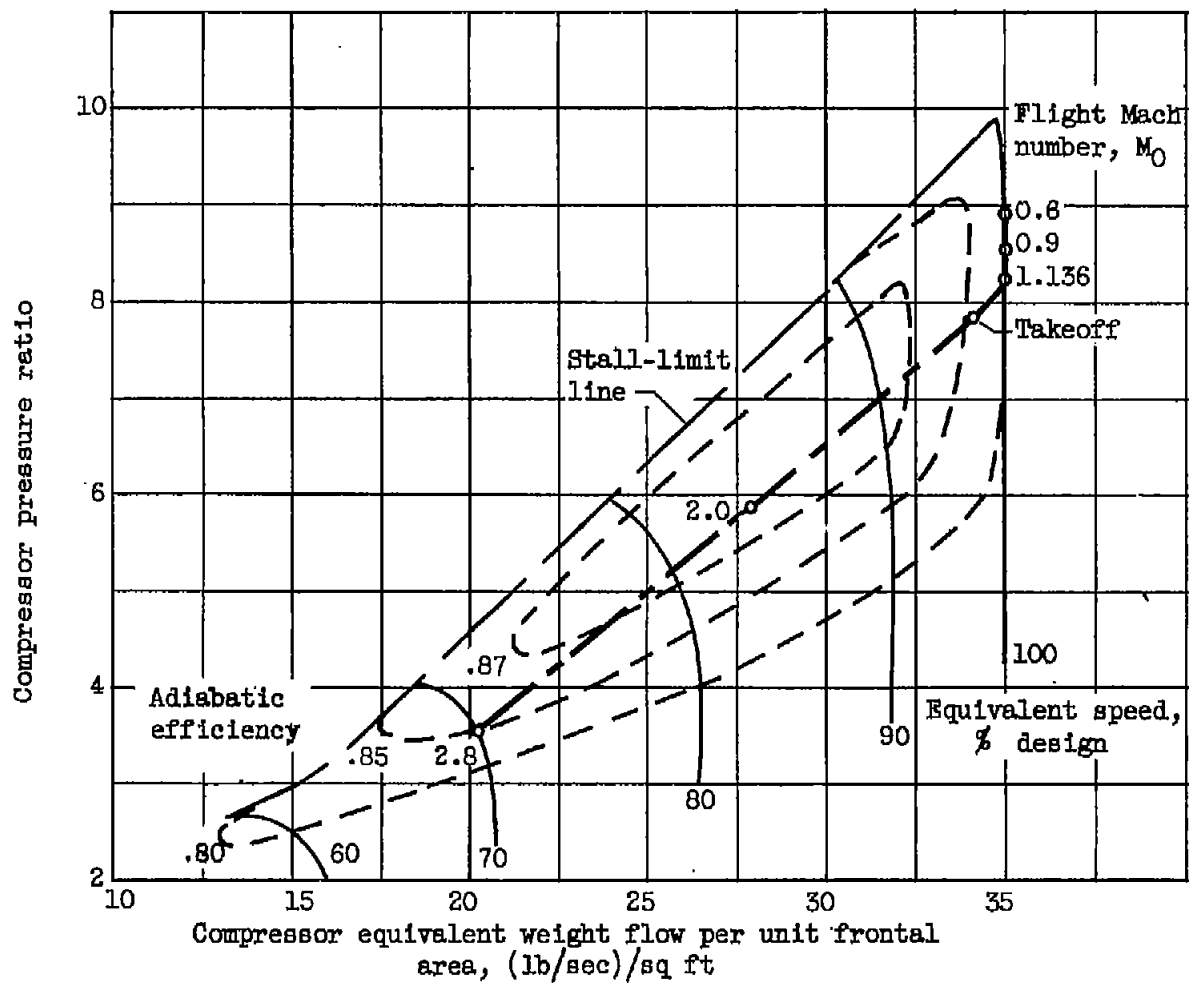
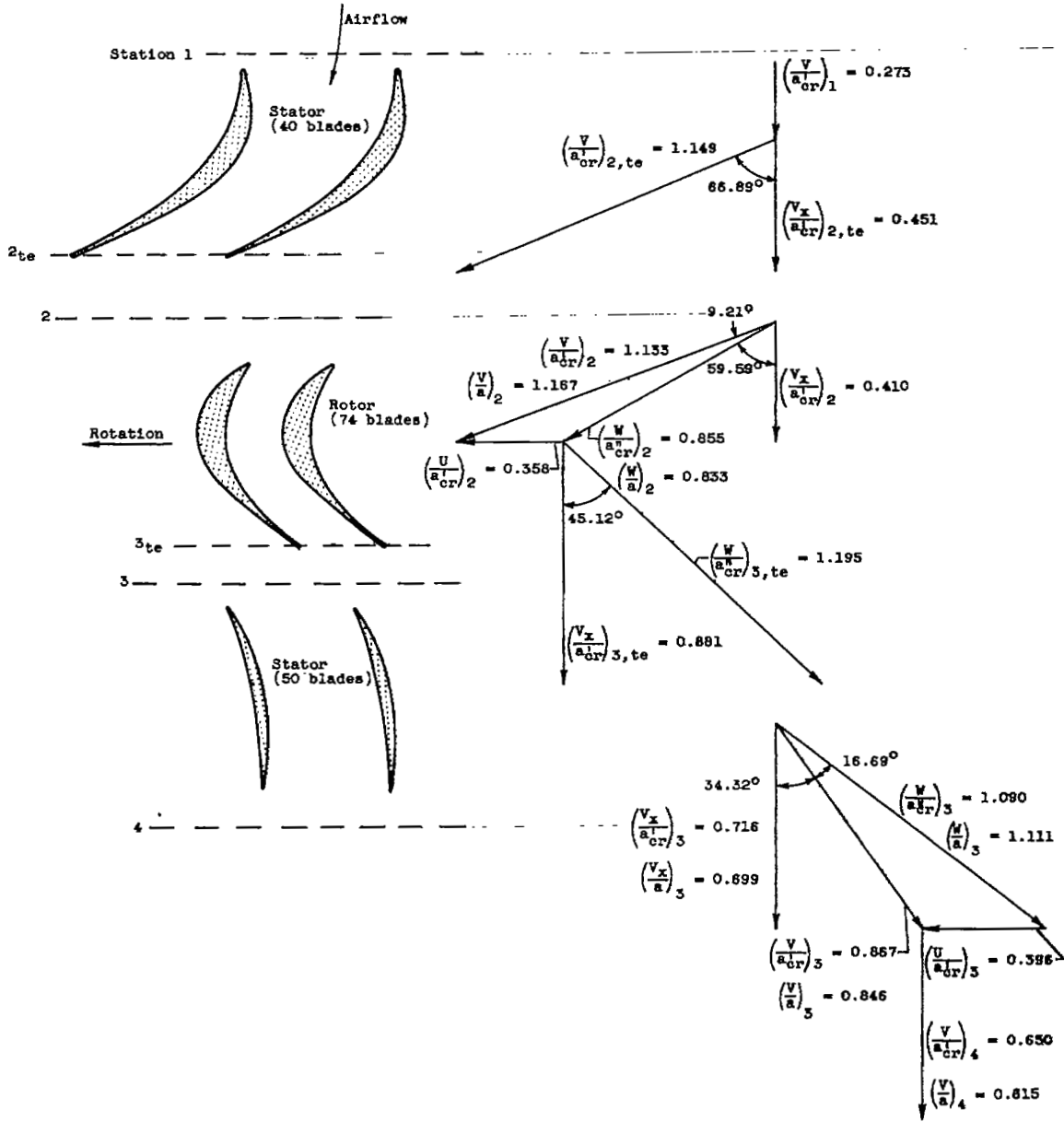


Figure 1. - Compressor operating line for takeoff and flight in the stratosphere.



(a) Hub.

Figure 2. - Design turbine velocity diagrams. Ratio of specific heats, 1.4.

4108

CM-4 back

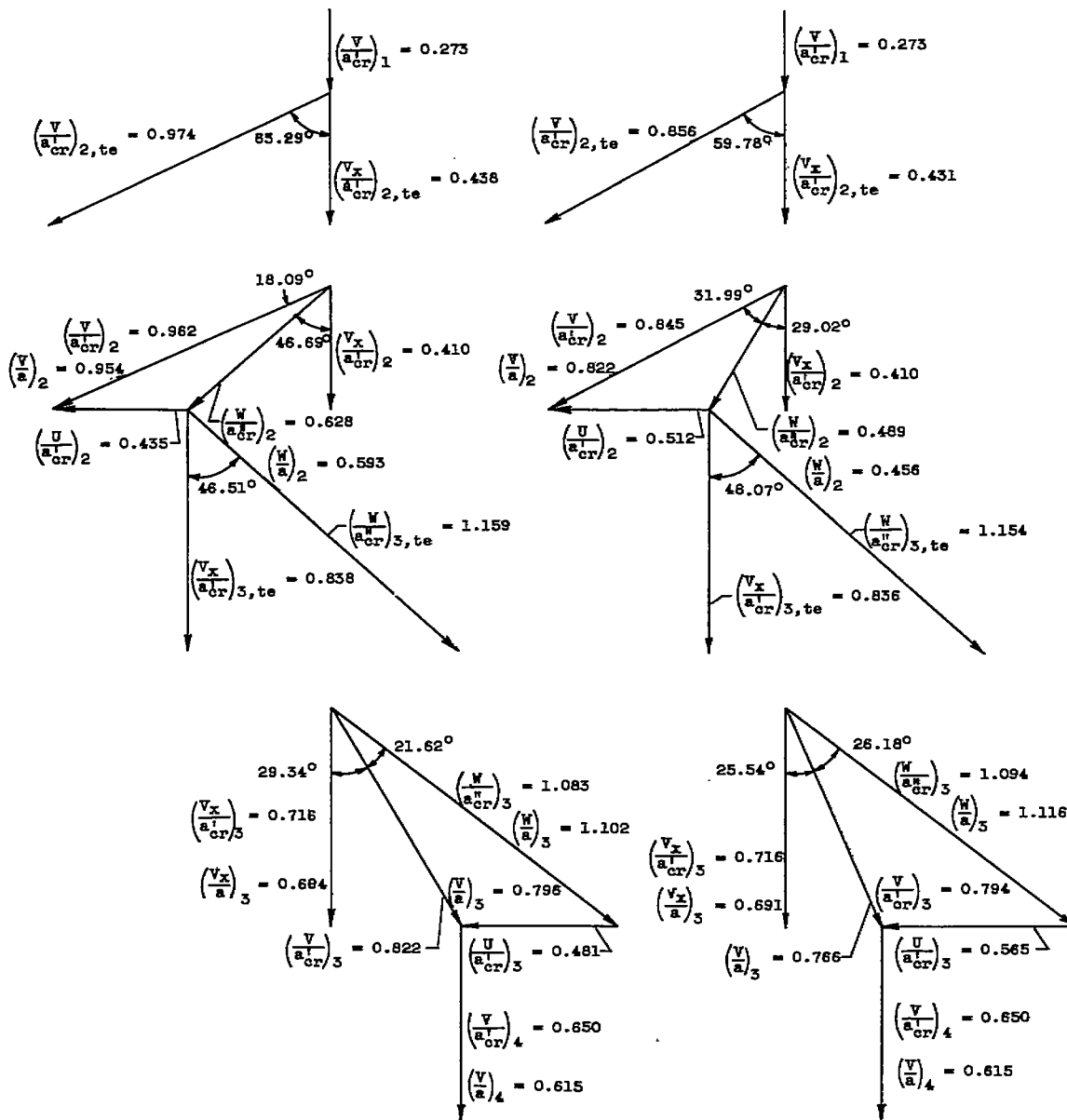
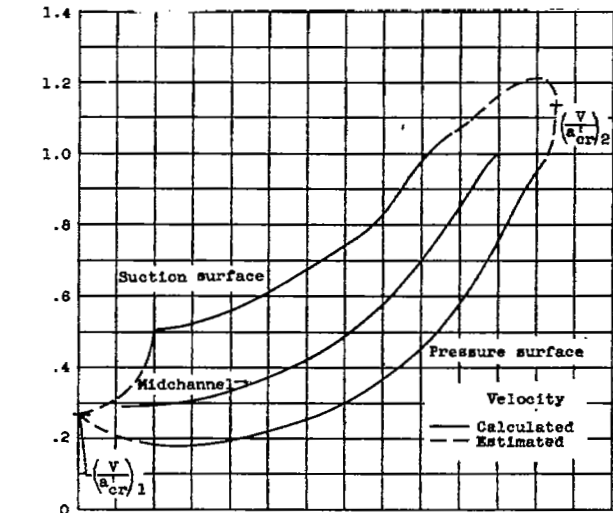
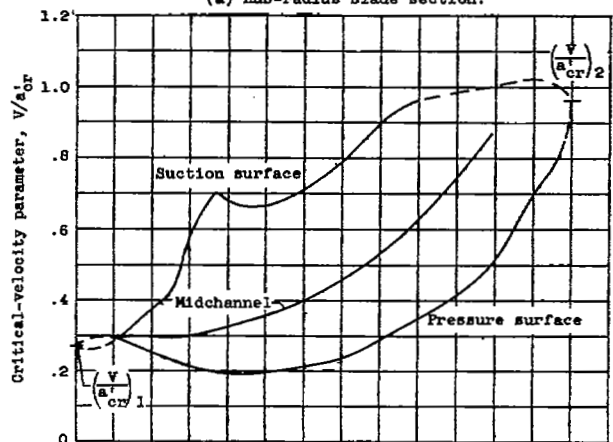


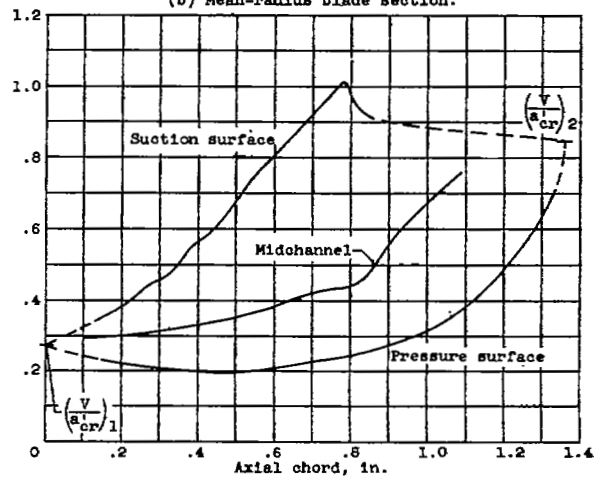
Figure 2. - Concluded. Design turbine velocity diagrams. Ratio of specific heats, 1.4.



(a) Hub-radius blade section.



(b) Mean-radius blade section.



(c) Tip-radius blade section.

Figure 3. - Design upstream-stator velocity distribution.

4108

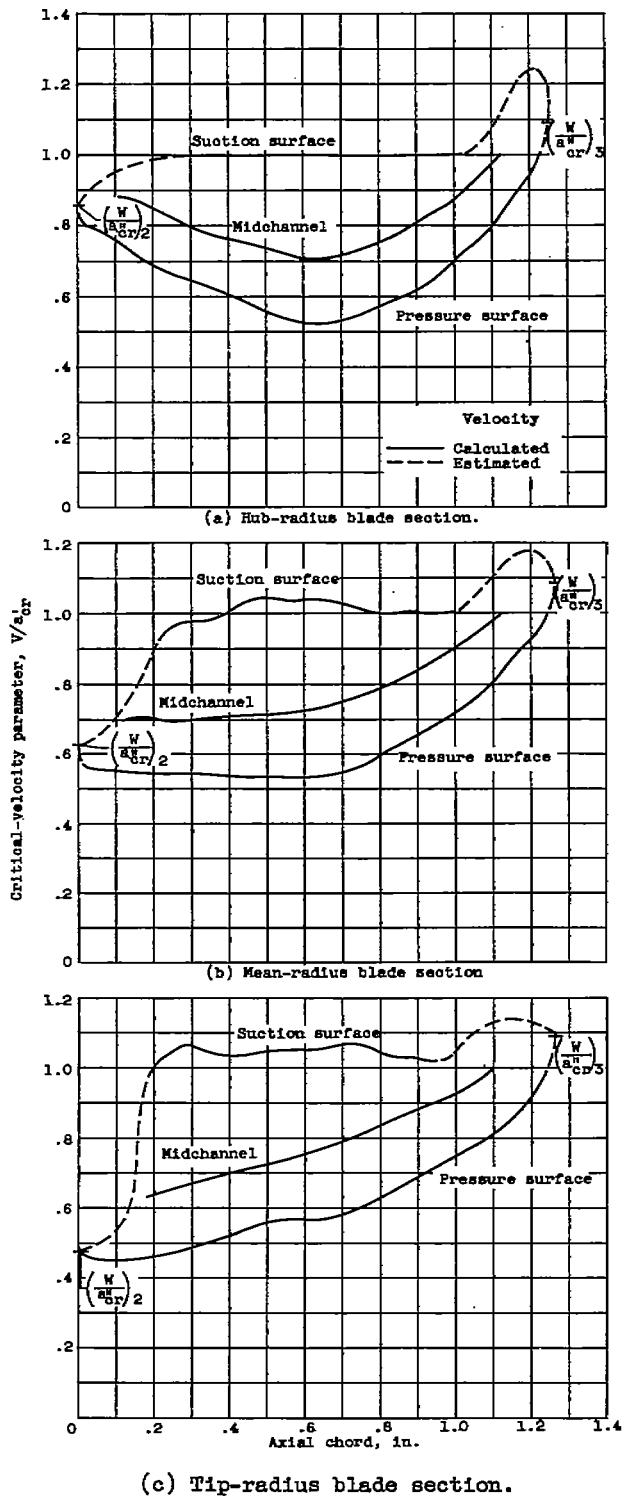
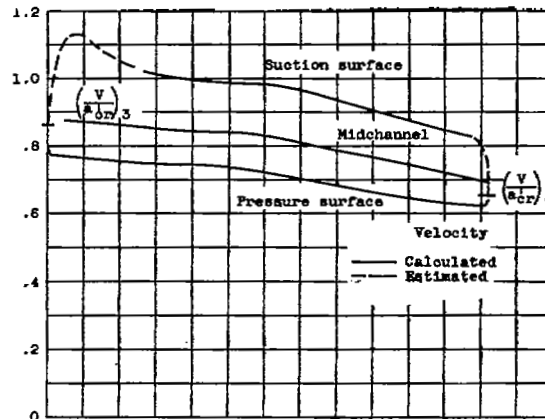
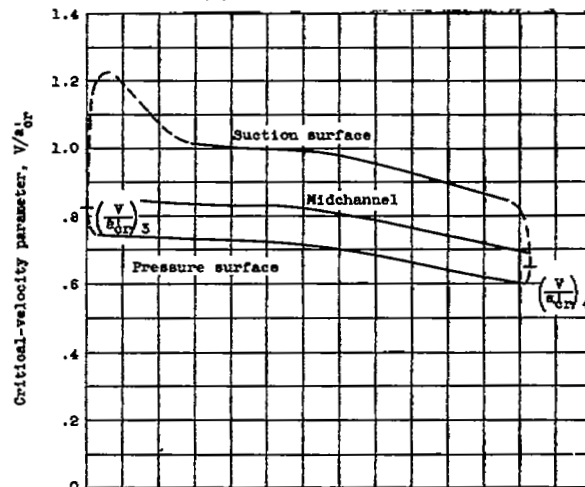


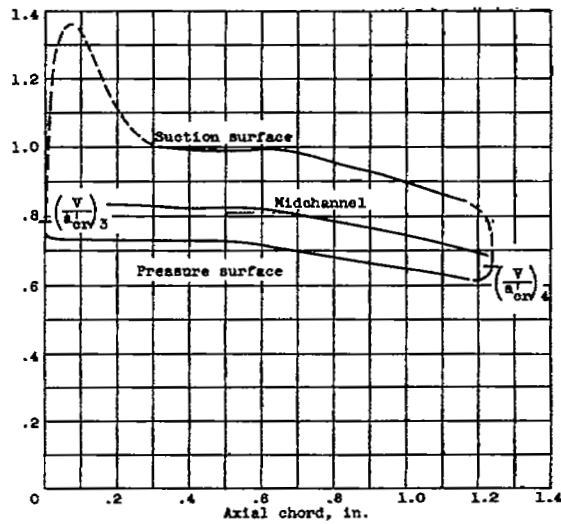
Figure 4. - Design rotor velocity distribution.



(a) Hub-radius blade section.



(b) Mean-radius blade section.



(c) Tip-radius blade section.

Figure 5. - Design downstream-stator velocity distribution

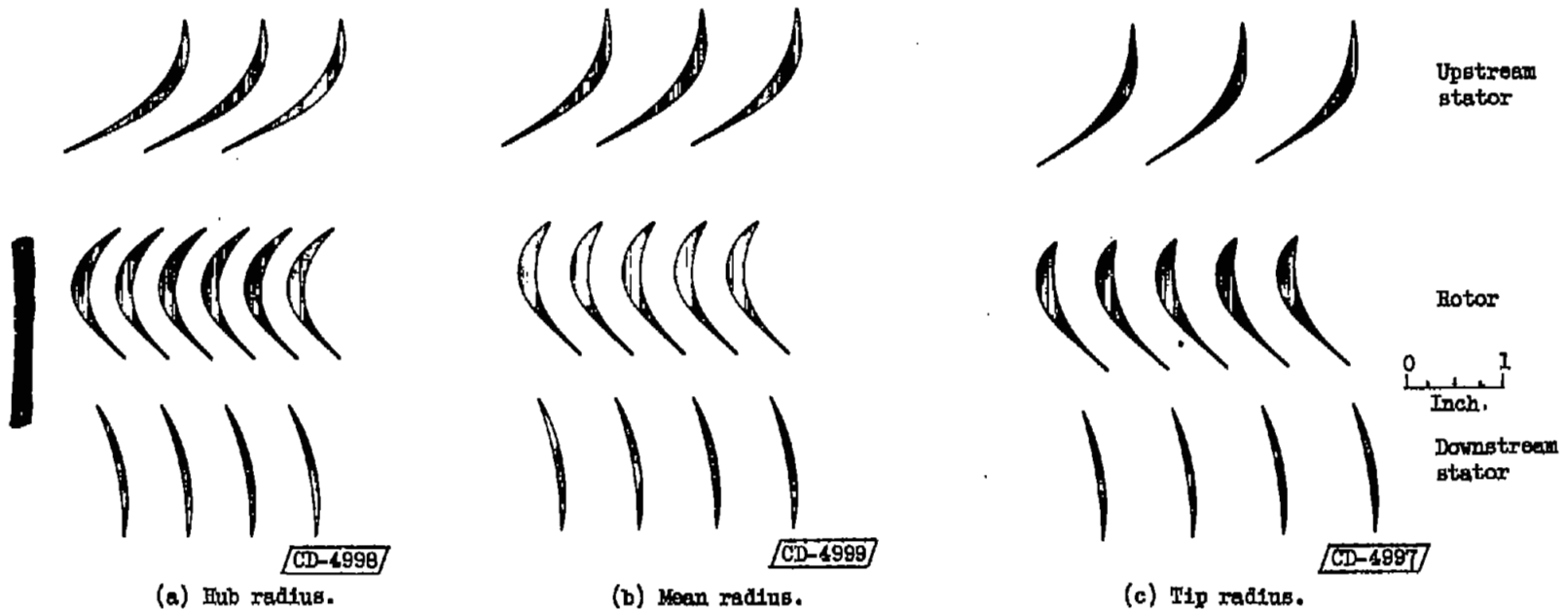


Figure 6. - Design turbine blade profiles.

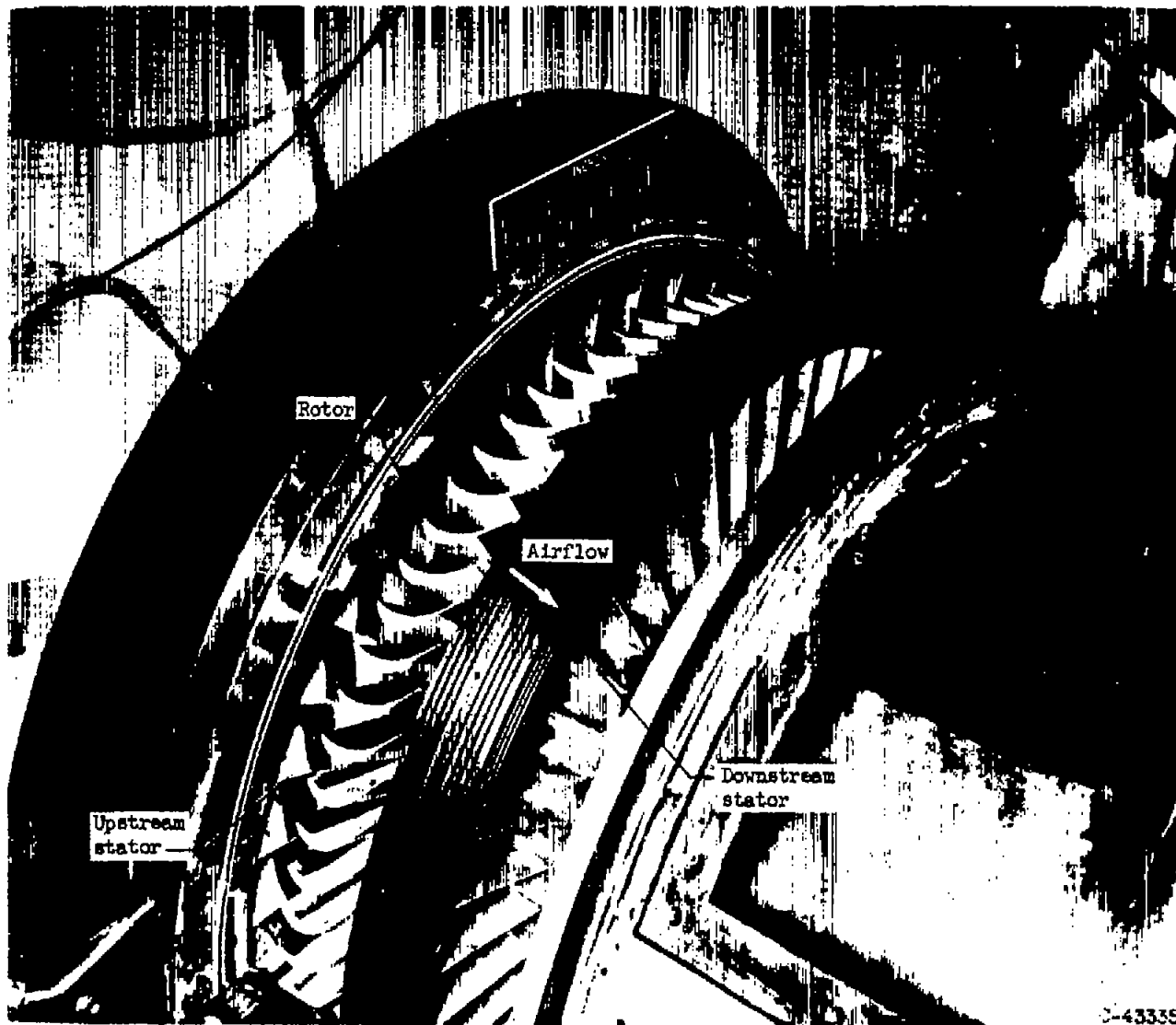


Figure 7. - Experimental turbine with top half of casing removed.

4108

CM-5

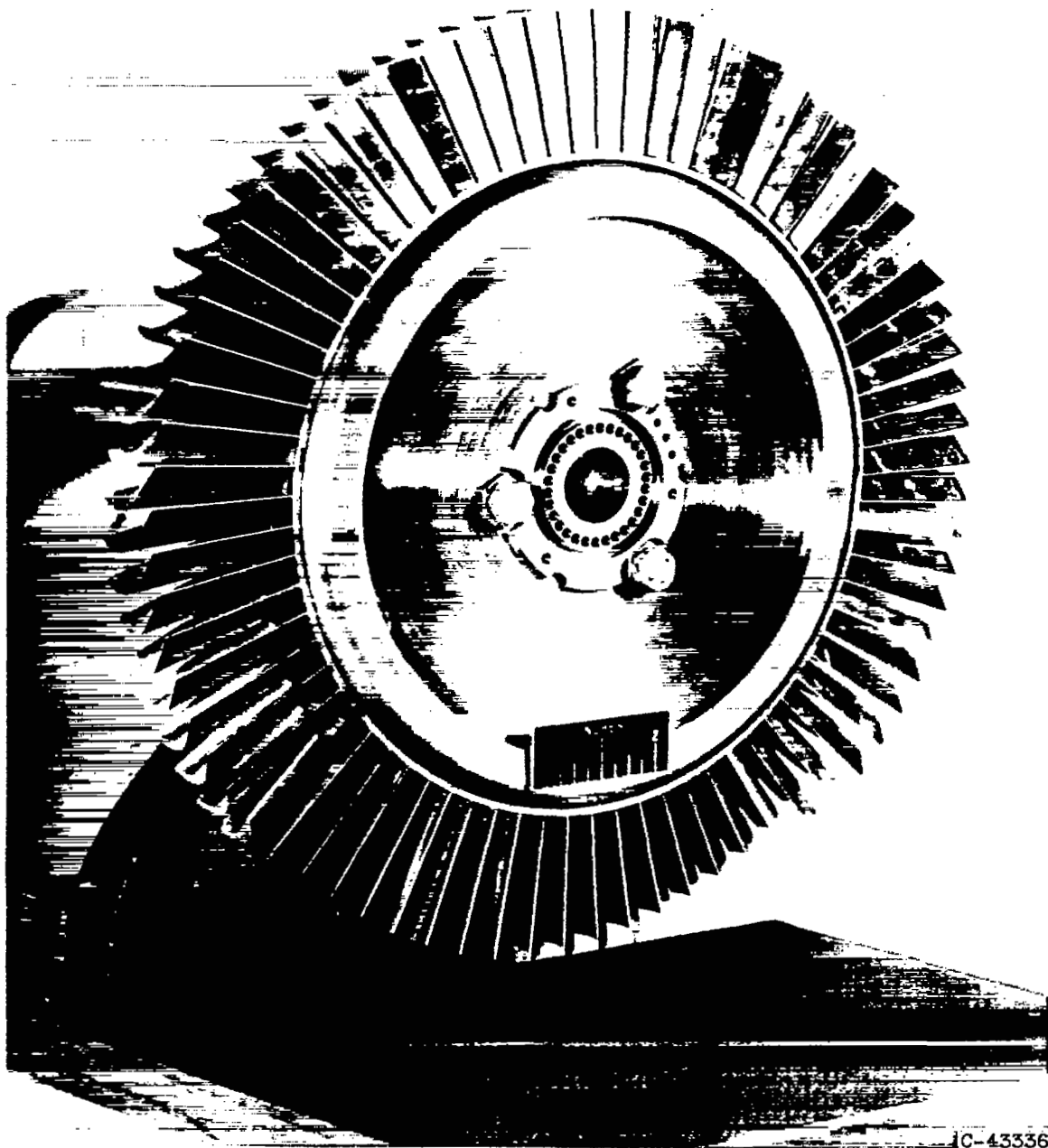


Figure 8. - Experimental rotor assembly.

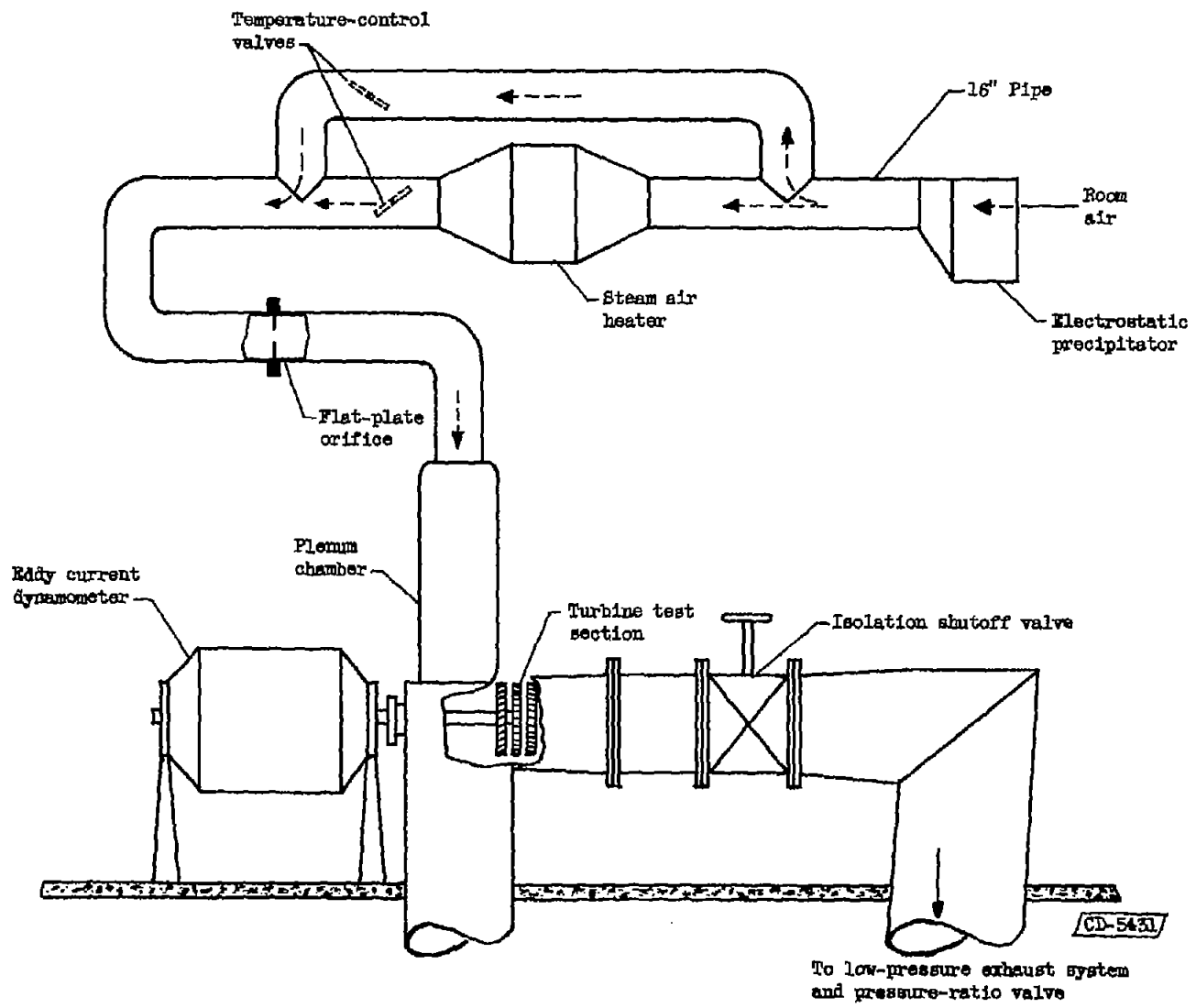
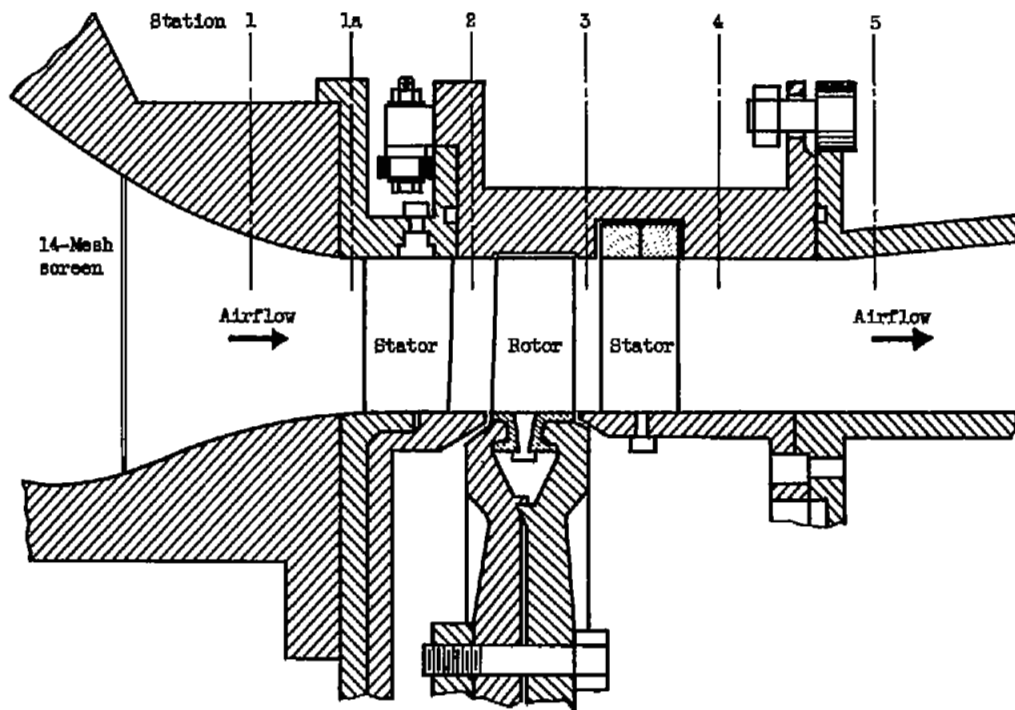
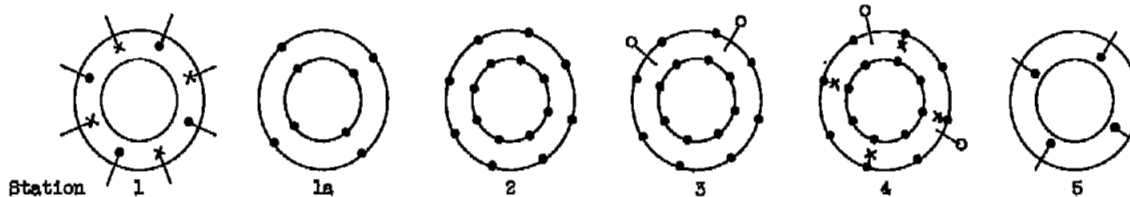
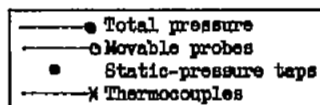


Figure 9. - Schematic sketch of arrangement of experimental equipment showing airflow path.

CONFIDENTIAL



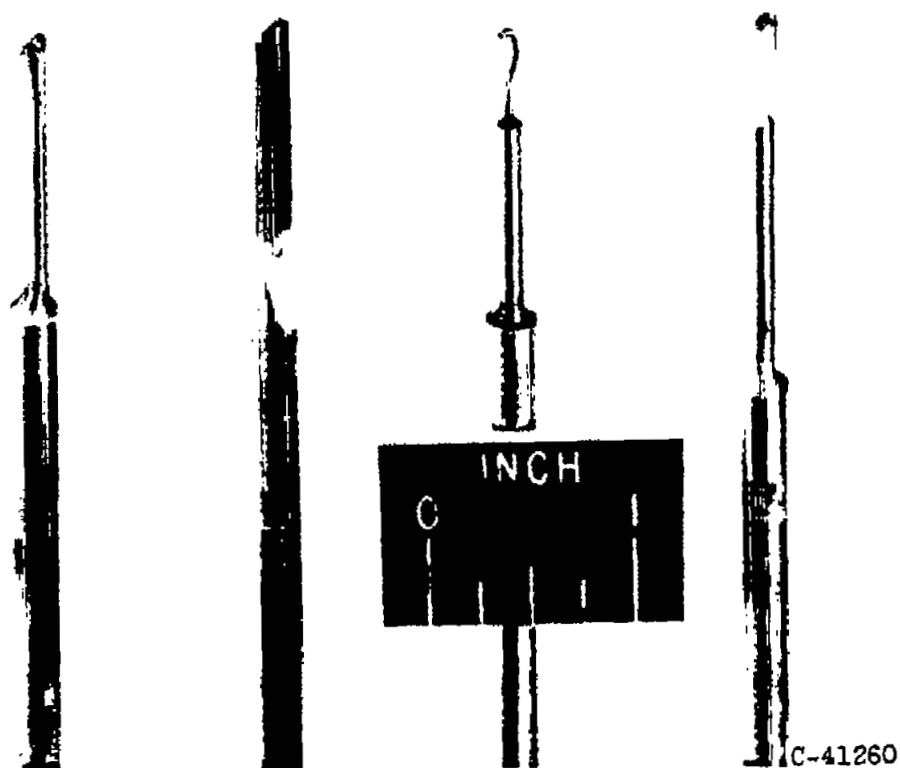
(a) Cross section of turbine showing measuring stations.



(b) Location of instrumentation at each axial station.

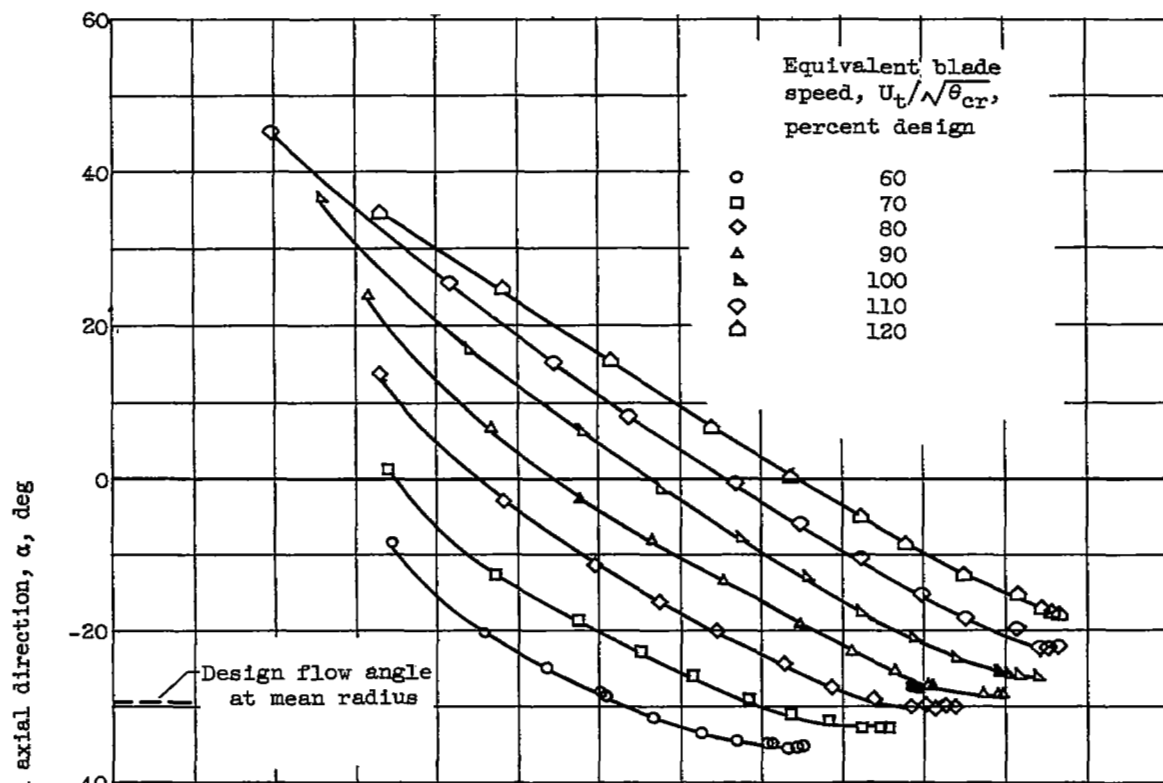
Figure 10. - Experimental turbine instrumentation.

CD-5430

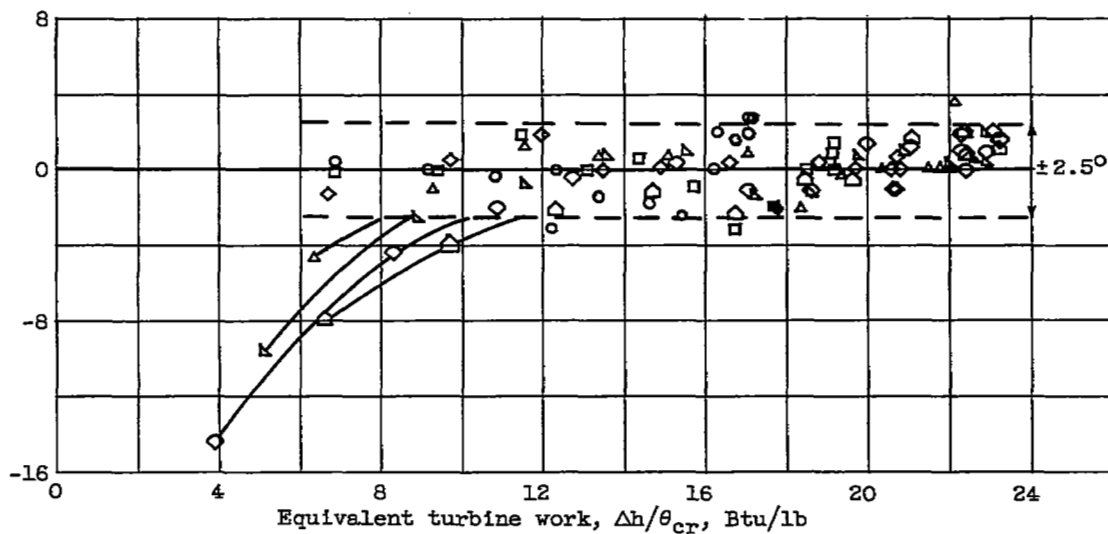


(a) Spike-type total-temperature thermocouple. (b) Static wedge angle probe. (c) Total-pressure probe. (d) Cobra angle probe.

Figure 11. - Typical instrument probes used for temperature, pressure, and flow-angle measurements.



(a) Flow angle at exit of rotor (station 3).



(b) Flow angle at exit of downstream stator (station 4).

Figure 12. - Variation of flow angle with turbine work for values of constant equivalent blade speed.

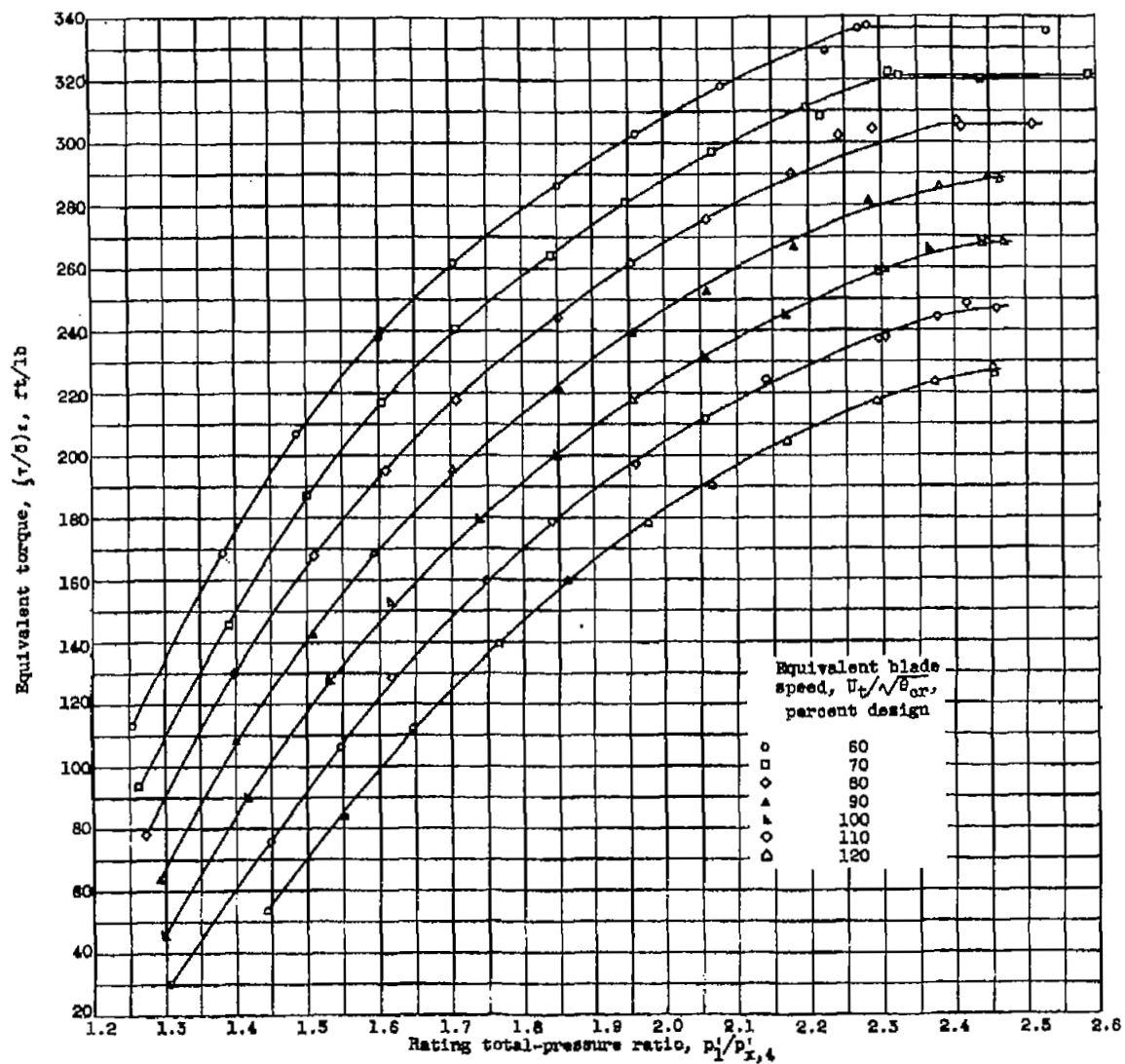


Figure 13. - Variation of equivalent torque with rating pressure ratio for values of constant equivalent blade speed.

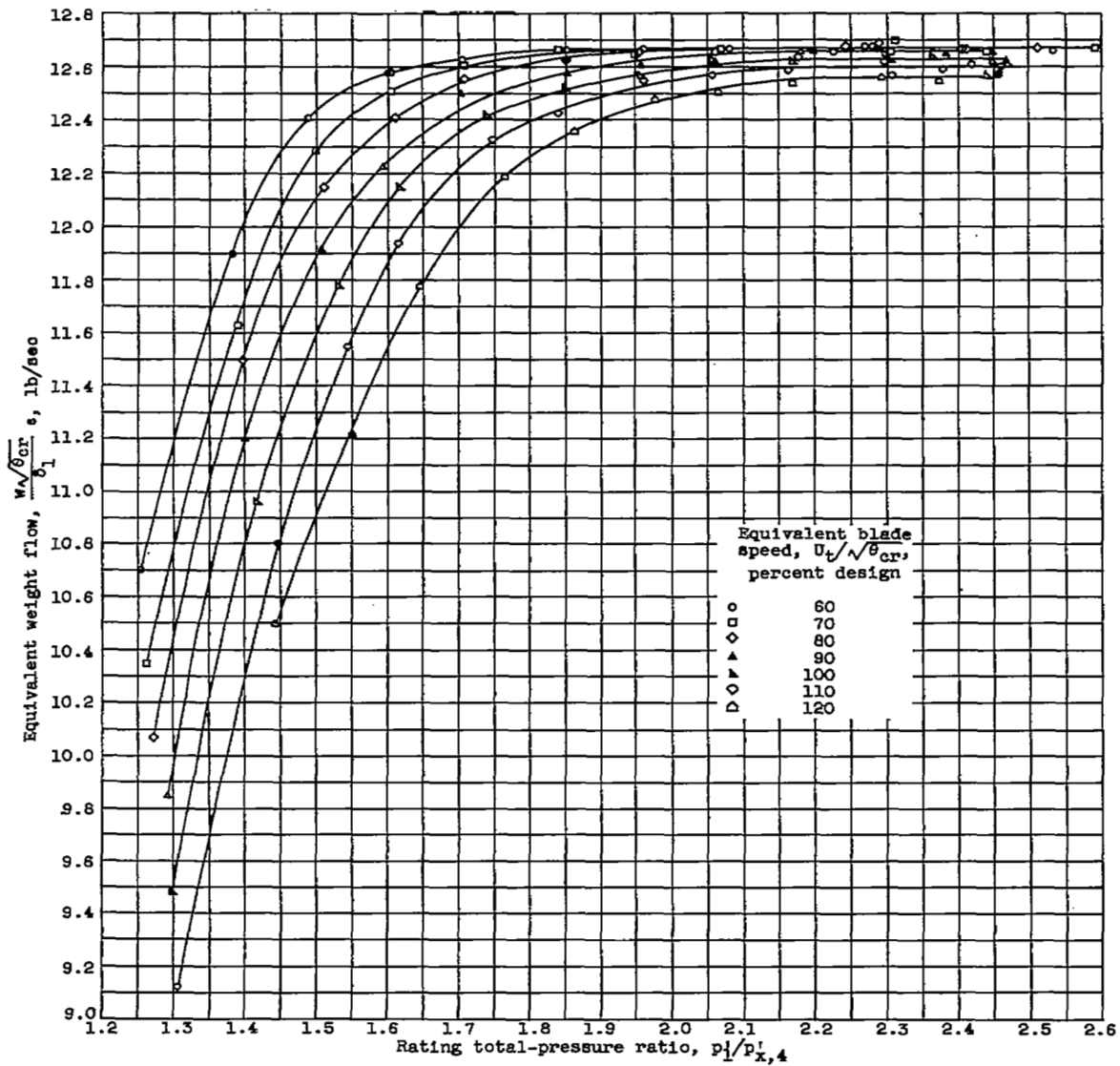
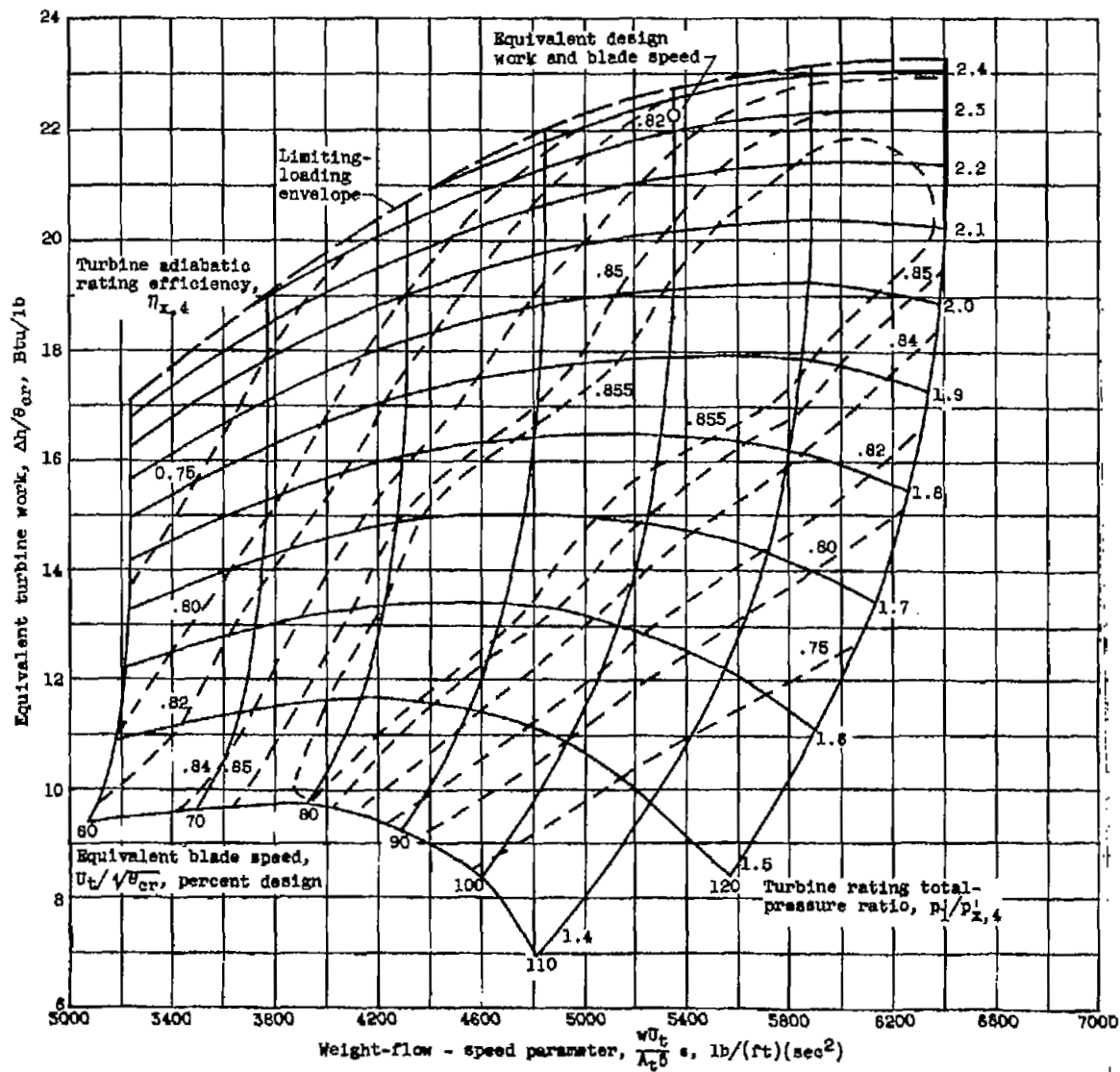
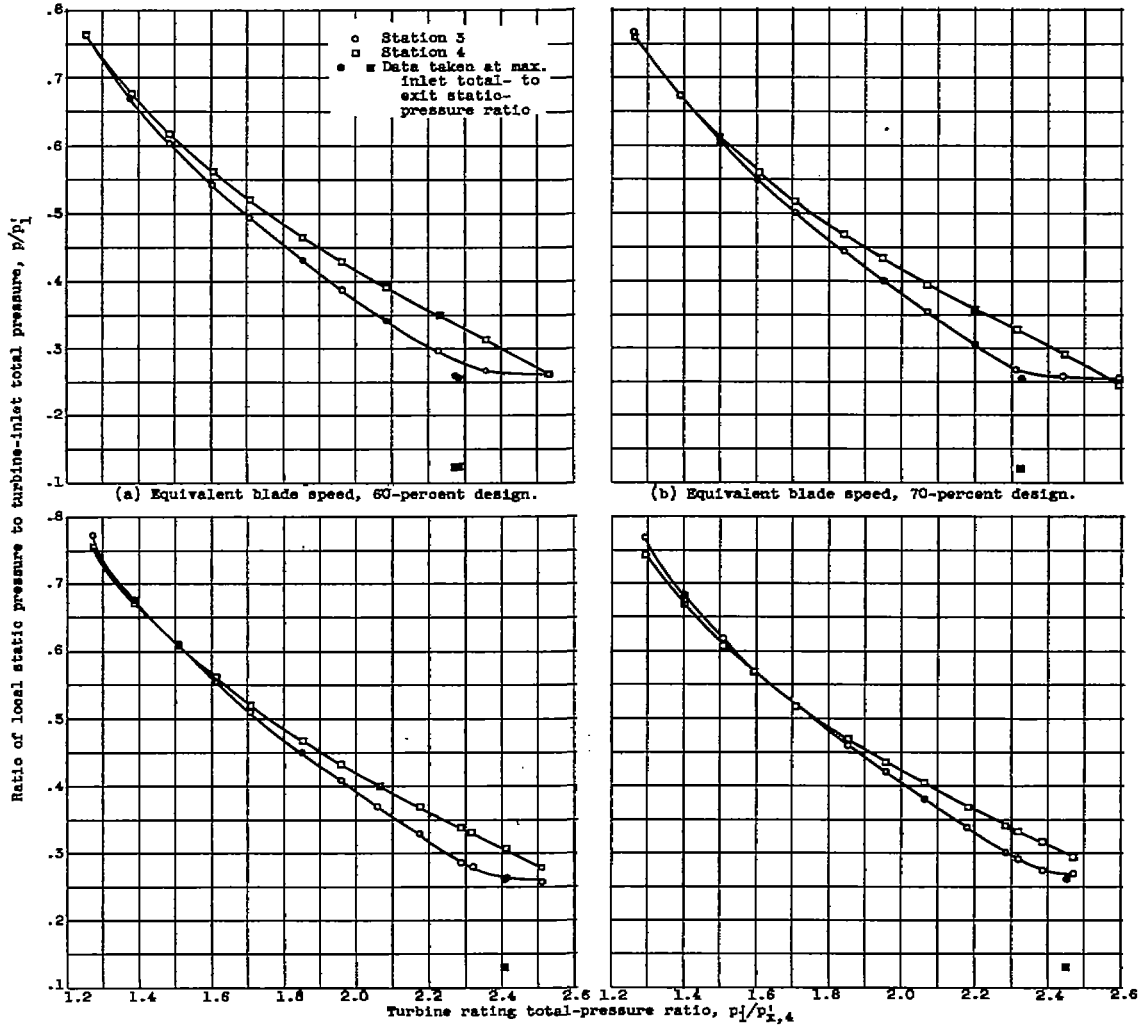


Figure 14. - Variation of equivalent weight flow with rating pressure ratio for values of constant equivalent blade speed.

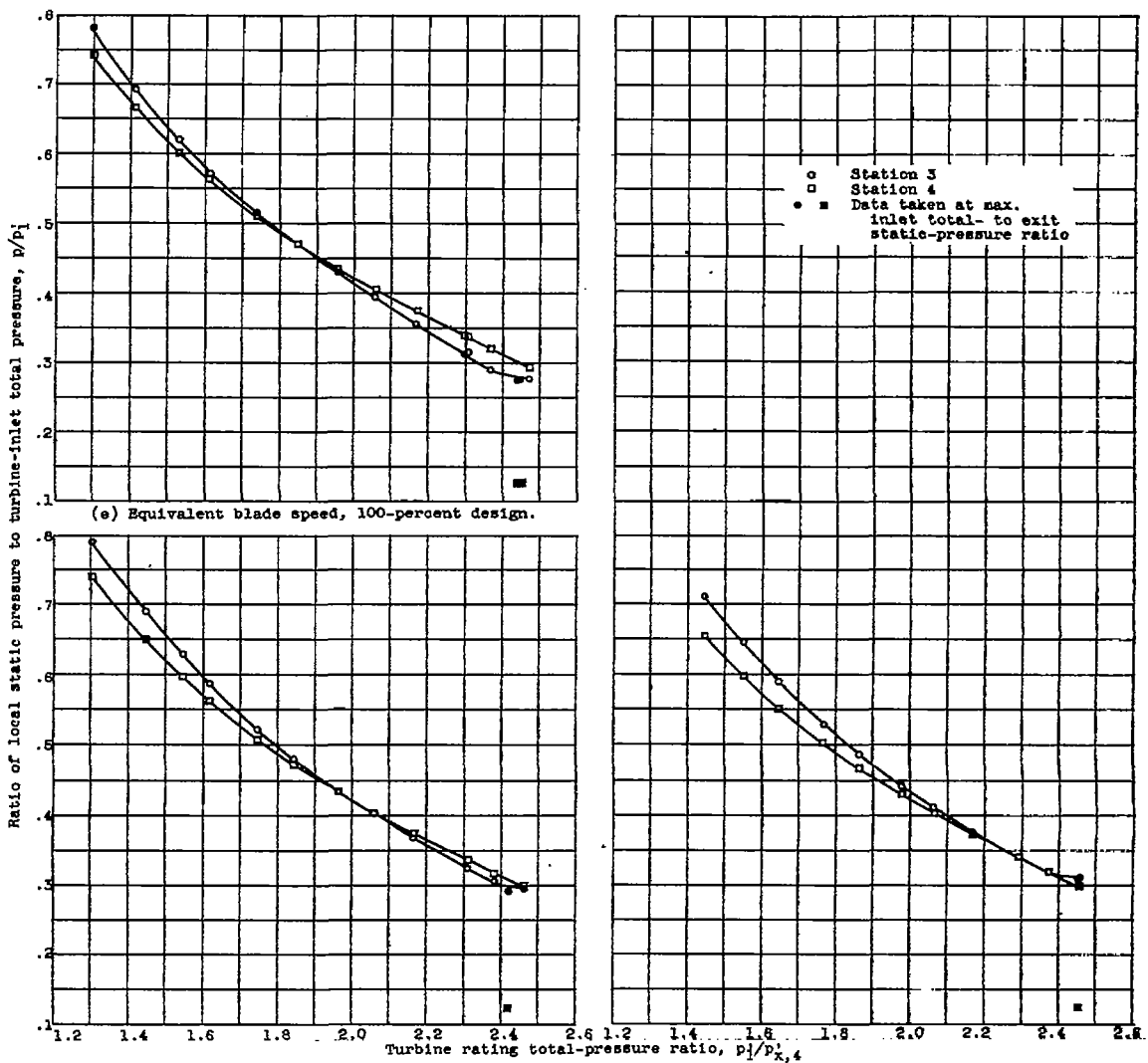


4108



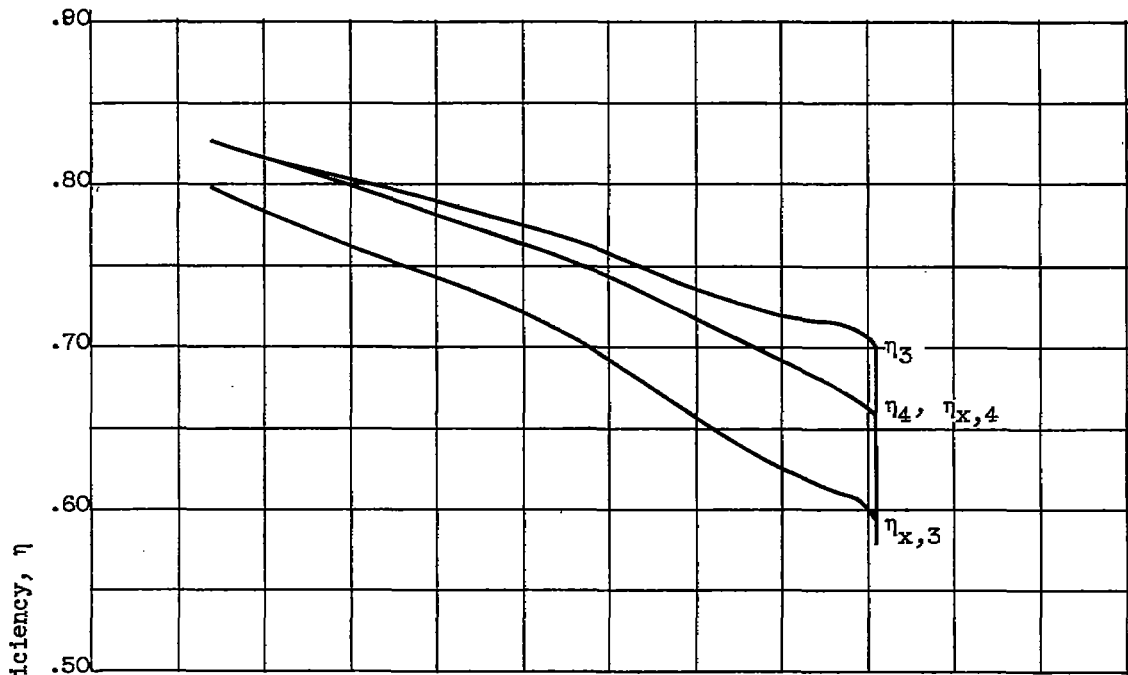
(a) Equivalent blade speed, 60-percent design. (b) Equivalent blade speed, 70-percent design. (c) Equivalent blade speed, 80-percent design. (d) Equivalent blade speed, 90-percent design

Figure 16. - Variation of static pressure with turbine rating total-pressure ratio at two axial measuring stations.

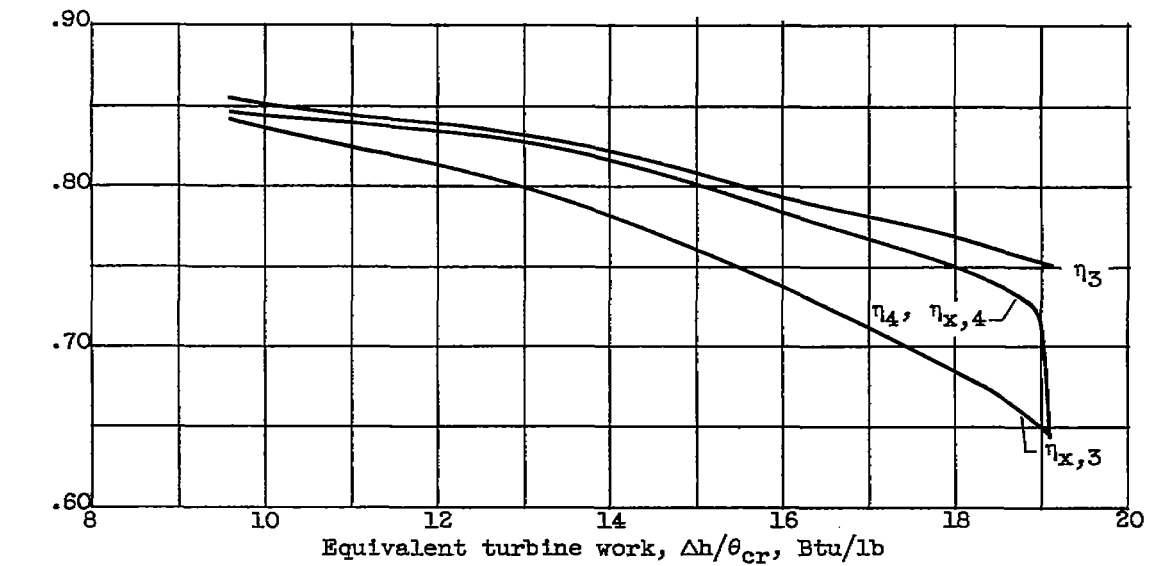


(f) Equivalent blade speed, 110-percent design. (g) Equivalent blade speed, 120-percent design.

Figure 16. - Concluded. Variation of static pressure with turbine rating total-pressure ratio at two axial measuring stations.

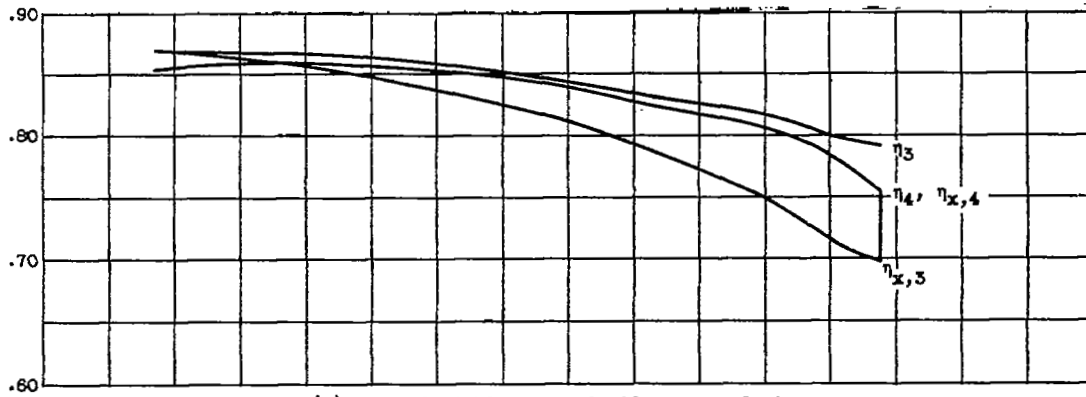


(a) Equivalent blade speed, 60-percent design.

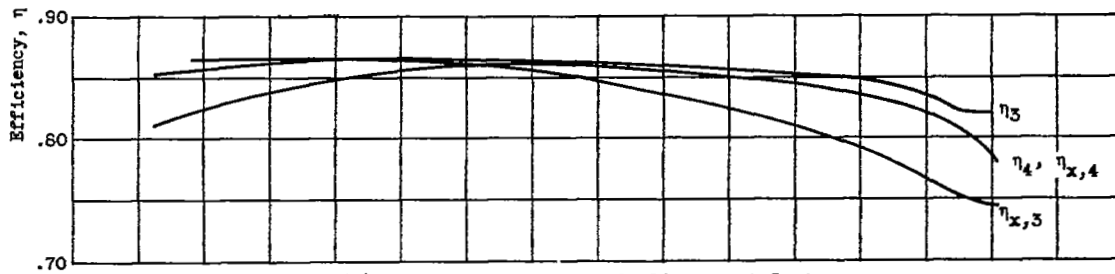


(b) Equivalent blade speed, 70-percent design.

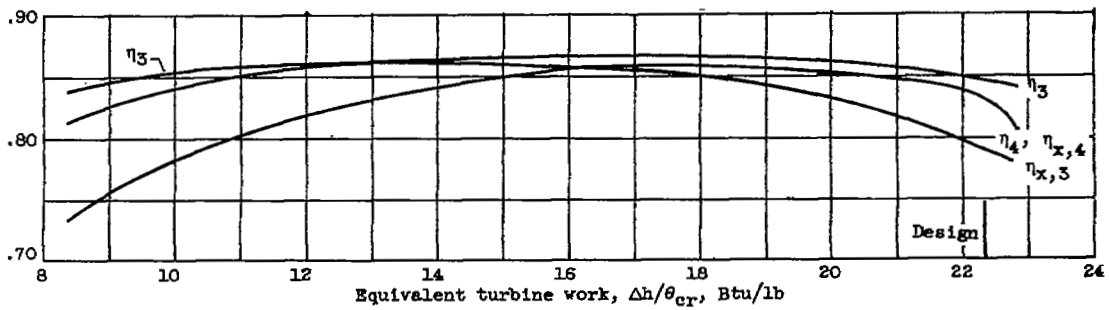
Figure 17. - Variation of turbine efficiency with turbine work output.



(c) Equivalent blade speed, 80-percent design.



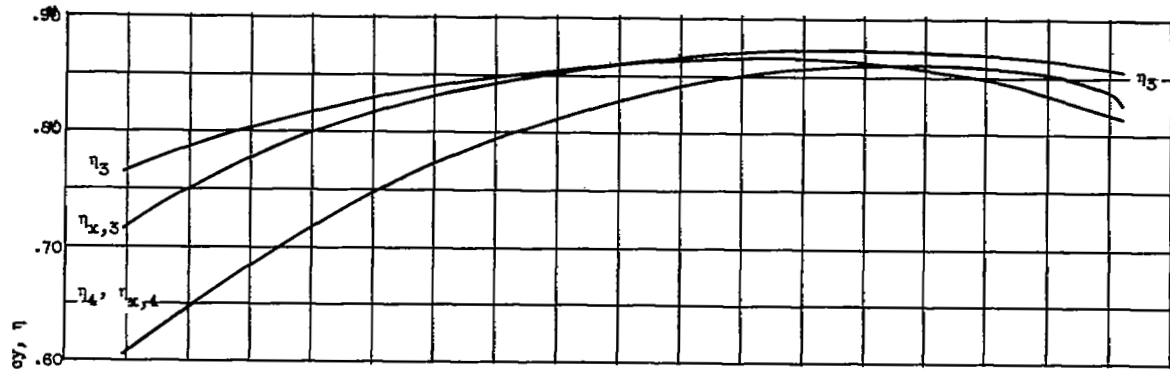
(d) Equivalent blade speed, 90-percent design.



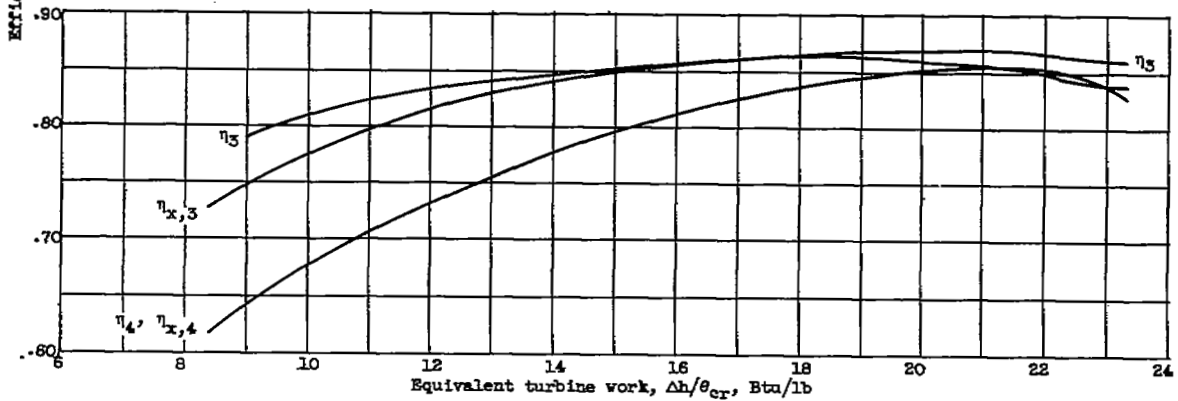
(e) Equivalent blade speed, 100-percent design.

Figure 17, - Continued. Variation of turbine efficiency with turbine work output.

4108



(f) Equivalent blade speed, 110-percent design.



(g) Equivalent blade speed, 120-percent design.

Figure 17. - Concluded. Variation of turbine efficiency with turbine work output.

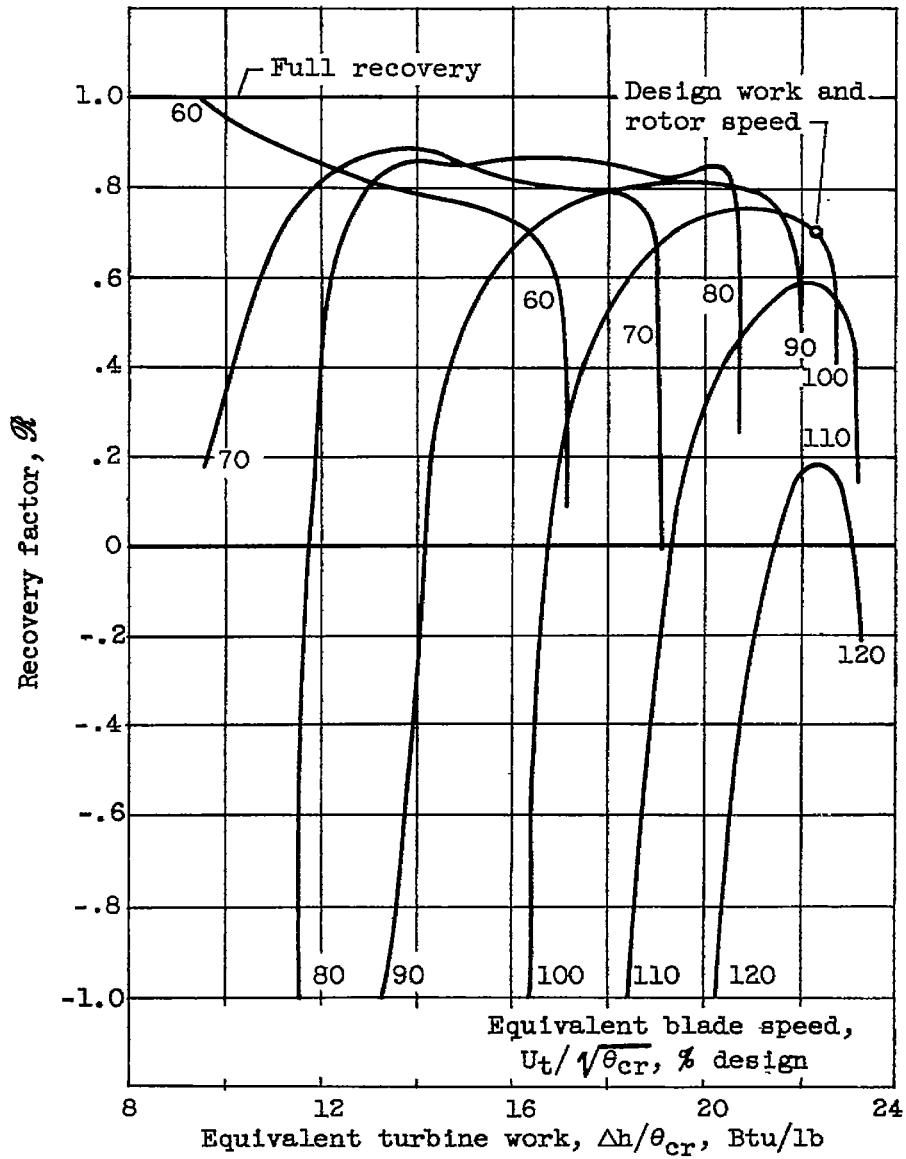


Figure 18. - Variation of recovery factor with turbine work output.

NASA Technical Library



3 1176 01436 0854

